Cent. Eur. J. Geosci. • 6(4) • 2014 • 588-613
DOI: 10.2478/s13533-012-0186-8

VERSITA

Central European Journal of **Geosciences**

Occurrence of Phlogopite in the Finero Mafic Layered Complex

Topical issue

Tommaso Giovanardi[1,2,3*], Maurizio Mazzucchelli[1,4†], Alberto Zanetti[4‡], Antonio Langone[4], Massimo Tiepolo[4], Anna Cipriani[1,5]

1 Dipartimento di Scienze Chimiche e Geologiche, Università degli Studi di Modena e Reggio Emilia, Largo S. Eufemia 19, 41121 Modena, Italy

2 Dipartimento di Scienze Della Terra e Dell'ambiente, Università degli Studi di Pavia, Via Ferrata 1, 27100 Pavia, Italy

3 Instituto de Geociências, Universidade de São Paulo, Rua do Lago, 563, Cidade Universitária, 05508-900 São Paulo, Brazil

4 Istituto di Geoscienze e Georisorse-C.N.R. U.O.S. of Pavia, Via Ferrata 1, 27100 Pavia, Italy

5 Lamont Doherty Earth Observatory of Columbia University, Palisades, New York, 10964, USA

Received 26 March 2014; accepted 30 June 2014

Abstract: Phlogopite-bearing lithologies are the main constituent of the Phlogopite-Peridotite unit of the Finero sequence and the result of pervasive migration of metasomatizing melts/fluids. Conversely, the presence of phlogopite within the associated Finero Mafic Complex, a mafic-ultramafic pluton intruded into the metamorphic basement of the Adria plate, is mentioned in literature as rare. Recent detailed fieldwork has evidenced the presence of two distinct phlogopite-rich ultramafic lithologies within the Amphibole-Peridotite unit of the Finero Mafic Complex, where phlogopite is always associated with amphibole. Field and petrographic features of these occurrences, as well as major- and trace-element mineral chemistry, are here presented to i) place constraints on the nature of the parent melt from which they have been generated and ii) to address their relationship with the other lithologies of the Finero Complex. We find that these rocks were formed by late melt migrations along shear zones under high-T conditions. The geochemical affinity of these lithologies is different to the tholeiitic-transitional affinity reported in literature for the Finero Mafic Complex. The enrichment in LREE, Th, U and Sr of the associated amphibole possibly suggests that these phlogopite-bearing lithologies are genetically related to the metasomatic events that have affected the Finero mantle massif.

Keywords: Phlogopite • Finero • Mafic Complex • Geochemistry • Ivrea-Verbano Zone

1. Introduction

The Finero Mafic Complex is a hydrous, layered pluton that intruded at the bottom of the Kinzigite Formation in the westernmost sector of the Southern Alps (Ivrea-Verbano Zone, IVZ). It consists of mafic, and subordinately ultramafic, rocks (comprising the following units: the Lay-

*E-mail: tommaso.giovanardi@gmail.com
†E-mail: maurizio.mazzucchelli@unimore.it
‡E-mail: zanetti@crystal.unipv.it

ered Internal Zone unit, the Amphibole-Peridotite unit and the External Gabbro unit) surrounding a completely metasomatized mantle massif (Figure 1; [1–9] and references therein).

The metasomatized mantle massif, named the Phlogopite-Peridotite unit (Ph-Pd; unit names and acronyms according to Siena & Coltorti [3]) by Cawthorn [1], is mainly composed of phlogopite-bearing amphibole harzburgite that contains secondary orthopyroxene, amphibole, phlogopite and clinopyroxene that segregated from metasomatizing melts/fluids. This indicates a pervasive recrystallization at mantle conditions [4, 7].

The Finero Mafic Complex is characterized by a great abundance of amphibole (i.e. hornblende to pargasite in composition, [3]) in all its units [1–3, 5, 6, 8, 9]; this is a major compositional difference when compared to the Mafic Complex forming the central IVZ, i.e. the Val Sesia Magmatic System [10–15].

For the Finero Mafic Complex, Siena & Coltorti [3] proposed a model of fractional crystallization starting from a hydrous transitional MORB. Lu et al. [5] suggested instead a hydrous tholeitiic to transitional MORB composition as parent melt. The same geochemical affinity was proposed by Zanetti et al. [8] for the parent melts of the External Gabbro unit (EG) within the Finero Mafic Complex. All authors agree that the amphibole was an early liquidus phase during the crystallization of the complex. Siena & Coltorti [3] suggest that its crystallization occurred after plagioclase segregation. Consistently, Zanetti et al. [8] document that, in the EG unit, amphibole crystallized as an interstitial phase after pyroxenes and plagioclase precipitation.

In contrast to the Finero mantle massif, the occurrence of phlogopite in the Finero Mafic Complex has not yet been properly recognized and studied. Only Coltorti & Siena [2] reported the 'rare' presence of this mineral within the Amphibole-Peridotite unit (Amph-Pd). Recent fieldwork led us to the recognition of abundant phlogopite that always occurs in association with amphibole within lithologies of the Amph-Pd unit.

The aim of this study is to provide a petrographic and geochemical characterization of the phlogopite-bearing lithologies of the Amph-Pd unit in order to constrain: i) the geochemical affinity of the parent liquid that has generated this peculiar mineralogical association; ii) the genetic relationships between the phlogopite-bearing rocks and the Finero Mafic Complex parent melt; and iii) the possible genetic link with the K-rich melts that migrated through the Finero mantle unit [4, 7, 16–23]. The characterization of these issues may provide fundamental information for the understanding of the controversial geodynamic evolution of the northern sector of IVZ.

2. Geological setting

The Finero mafic-ultramafic sequence outcrops in the western Southern Alps in a lens about 12 km long and ~3 km thick, through the Vigezzo – Cento Valli Valley and the Cannobina Valley (Figure 1). It is the northernmost part of the Ivrea-Verbano Zone (IVZ), a geological unit composed of mafic-ultramafic intrusions and associated mantle peridotites that were emplaced in the crystalline basement of the Southern Alps before the Jurassic opening of the Ligurian branch of the Neo-Tethys.

The Finero mafic-ultramafic sequence consists of a metasomatized mantle massif [4, 7, 16–20] surrounded in an antiformal structure by a hydrous layered complex (the Finero Mafic Complex; [1–3, 5, 6, 8]), which intruded the crystalline basement of Southern Alps (the Kinzigite Formation). According to Zanetti et al. [8], the Finero Mafic Complex is divided into three main units: i) the Layered Internal Zone (LIZ), which is stratigraphically the lowest unit and is in tectonic contact with the underlying mantle massif; ii) the Amphibole-Peridotite (Amph-Pd); and iii) the External Gabbro (EG), which represents the uppermost unit and is in magmatic contact with the Kinzigite Formation. The mantle massif at the core of the antiformal structure is referred to as the Phlogopite-Peridotite unit (Ph-Pd hereafter).

The Ph-Pd unit is a completely metasomatized mantle peridotite [4, 7, 16–23] that formed by the pervasive-to-channeled migration of a metasomatizing melt/fluid within dunite and harzburgite bodies, accompanied by the pervasive crystallization of secondary amphibole, phlogopite, orthopyroxene and clinopyroxene. The harzburgites are associated with phlogopite-bearing amphibole websterites, whereas the dunites contain chromitite layers, phlogopite-bearing amphibole websterites, pegmatoidal websterite pods and mono-mineral phlogopite veins [7, 17, 18, 20]. The metasomatizing melts/fluids contained abundant crustal component(s), as revealed by trace-element and isotope data [4, 7, 17–22].

Additionally, the Ph-Pd unit experienced late porous flow percolation of different kind of melts along small channels or in opening fractures, with segregation of apatite, dolomite and sapphirine, together with amphibole and phlogopite [7, 17, 20–23].

The contact of the Finero Mafic Complex with the Ph-Pd unit is always tectonic and is marked by a one decimeter-thick ultra-mylonite. Given this type of contact and their contrasting lithologies, the Mafic Complex and the mantle massif probably had independent geological evolutionary paths.

The LIZ Unit (with a thickness ranging from 70 to 120 m, [3]) consists mainly of garnetiferous hornblendites, associ-

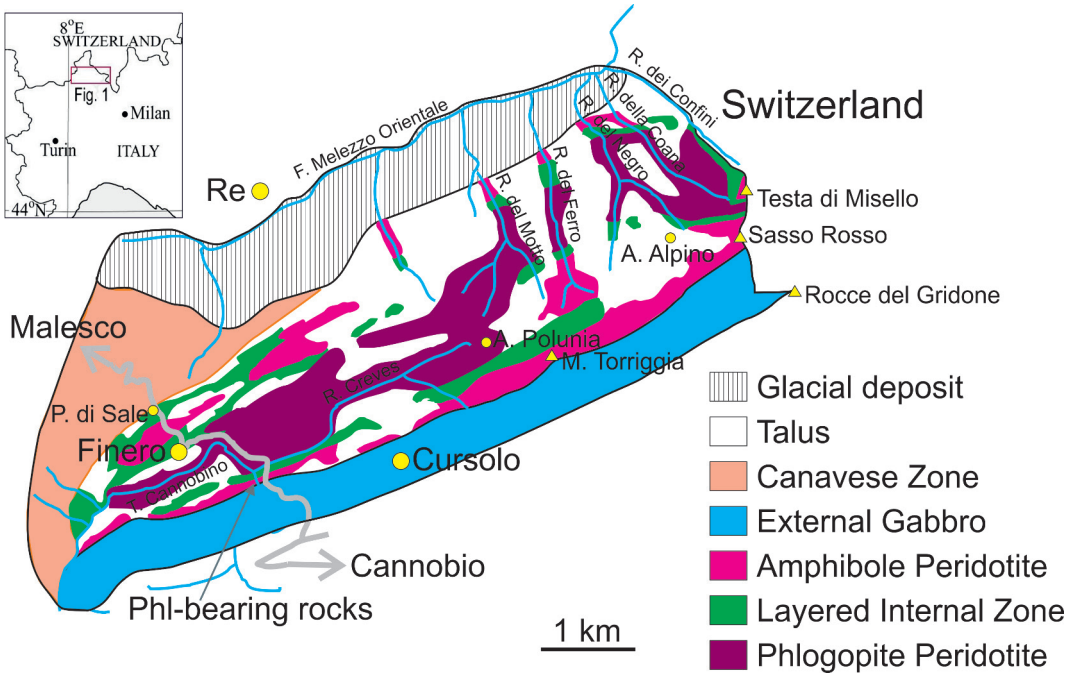

Figure 1. Geological map of the Finero area, modified after Mazzucchelli et al. [44].

ated with garnet-bearing amphibole gabbros, anorthosites, pyroxenites and peridotites, in decreasing order of abundance. In the southern zone of the LIZ, the layers are spatially limited (cm to m thick), often faulted and intersected by boudinate structures. In the northern zone of the LIZ the sequence is slightly different: peridotites and anorthosites are rare, and gabbros are more abundant than hornblendites. Near the contact between LIZ and Amph-Pd some gabbros contain sapphirine [24, 25].

The contact between LIZ and Amph-Pd is gradational, and is defined by a progressive increase of peridotitic and pyroxenitic layers with a decrease in abundance of the LIZ lithologies.

The Amph-Pd Unit is formed by amphibole-bearing cumulate peridotites (dunites, wehrlites and subordinate lherzolites, [3]), pyroxenites and hornblendites. The latter occur as bands, lenses and pods, sometimes with a pegmatitic texture and amphibole crystals longer than 1 m. The thickness of this unit varies from 200 to 300 m. The rock layers can be up to few meters thick and often are laterally limited and dismembered in boudinate structures. Pyroxenites are concentrated at the base and top of the unit: sulphides can occur near the contact with the EG unit. Peridotites predominate in the central part of the unit, where small layers and/or lenses of Cr-rich spinel are locally present. The Amph-Pd unit shows evidence of re-equilibration processes, namely triple junctions with 120° angles at crystal boundaries, and exhibits a smaller grain size relative to the analogue Ph-Pd unit. Sometimes olivine, orthopyroxene, and more frequently amphibole, are pecilitic with inclusions of green spinel; spinel is present also as an interstitial phase. Phlogopite was first reported in this unit by Coltorti & Siena [2].

The contact between the Amph-Pd and the EG is frequently affected by faults. When gradational, it is defined by a close alternation of layers of peridotite, hornblendite and gabbro, 20 cm to 1 m thick. The contact with the W zone of the body is sharp.

The EG unit is 400 to 500 m thick and consists mainly of amphibole diorites and gabbros, with minor pyroxenites and anorthosites, enriched in magnetite and ilmenite compared to the other rocks from the Finero area. The EG unit contains lenses of granulite-facies metasediments, which increase and become abundant towards the gradational contact with the Kinzigite Formation [1, 3, 5, 6, 26].

3. Occurrence of phlogopite in Amph-Pd

The occurrence of phlogopite as a rare phase in the Amph-Pd unit of the Finero Mafic Complex was first reported by Coltorti & Siena [2]. However, they neither describe its textural relationships, nor provide geochemical analyses of the phlogopite and associated mineral phases.

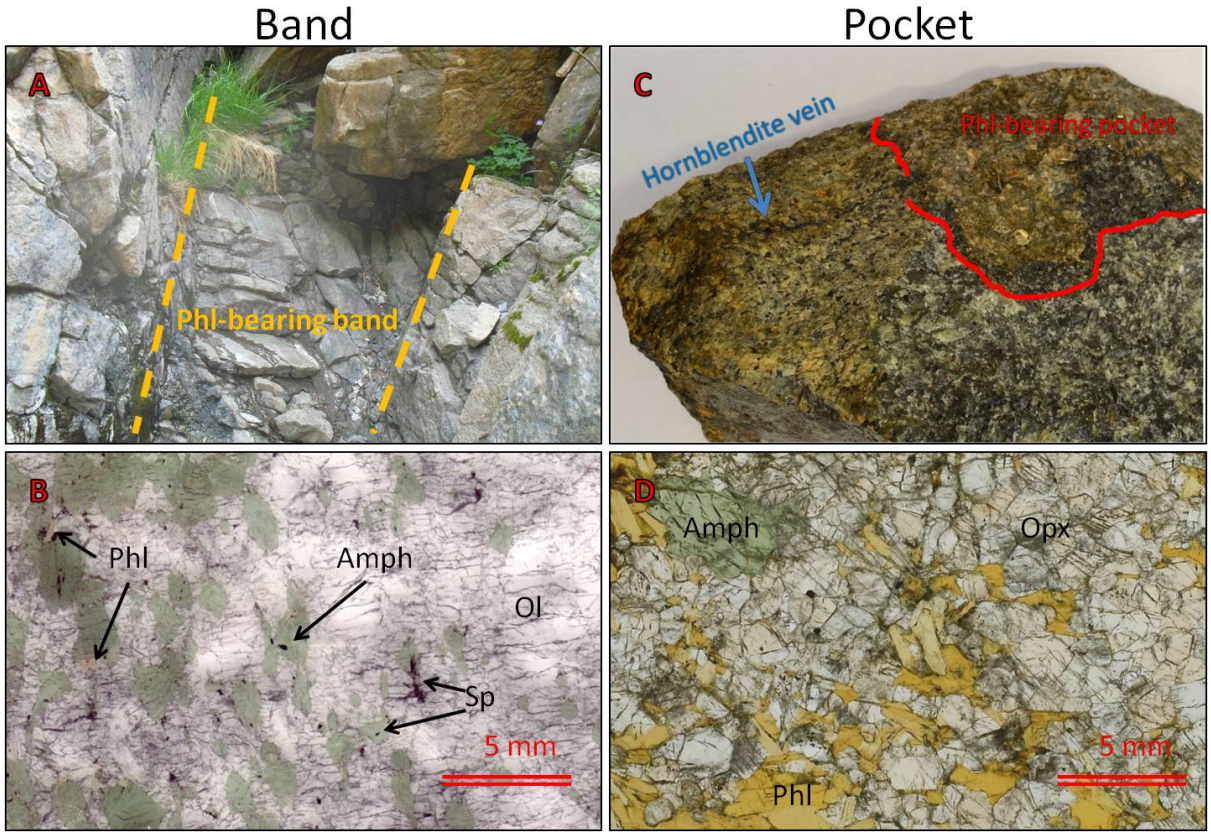

Figure 2. A) Picture of the phlogopite-bearing band within the Amph-Pd; borders of the outcrops are highlighted with an orange dashed line. B) Detail of the texture of the phlogopite-bearing band peridotite; abbreviations are used for minerals: Amph (Amphibole), Phl (Phlogopite), Sp (Spinel) and Ol (Olivine). C) Sample of the phlogopite-bearing pocket and associated hornblendite vein and host peridotite; borders of the pocket are highlighted by a red line. D) Detail of the pocket texture; abbreviations are used for minerals: Amph (Amphibole), Phl (Phlogopite) and Opx (Orthopyroxene).

Recent fieldwork has allowed us to distinguish two different phlogopite-bearing rocks within the Amph-Pd unit of the Finero Mafic Complex. Phlogopite occurs in two assemblages: i) in peridotite bands and/or lenses as a pervasive phase mainly associated with amphibole; and ii) in a late vein associated with an orthopyroxenite pocket.

The phlogopite-bearing peridotite outcrops after the masonry bridge on the eastern side of the Cannobino River (Figure 2a; 46° 06′ 16″ N–08° 32′ 41″ E). This peridotite is 2–3 m thick and about 15–20 m above the LIZ-Amph-Pd contact (i.e. to the south, because of the almost vertical dip of the rocks). Due to the vegetation cover, it is not possible to determine the actual extension of the outcrop and its geometry remains, therefore, unknown. Hereafter, for simplicity, we consider this occurrence of phlogopite-bearing peridotite as a band. The band is formed by a dunite matrix with elongated crystals of olivine (from a few mm up to 1 cm), often showing kink-banding. Black spinel commonly occurs as an accessory phase but locally reaches modal abundances of up to 4% by volume. Recrystallization zones in the dunite assemblage are common, where small olivine neoblasts with mosaic texture occur. Pervasive green amphibole is present in a modal abundance from 2 to 40% by volume. Amphibole is a late-stage crystallization phase, represented either by small crystals (2–5 mm), mainly located in interstitial positions, or by larger grains (5–10 mm) located within and at the border of the recrystallization zones. The phlogopite is present as an accessory phase. The phlogopite flakes are mainly associated to the amphibole grains, but single crystals in interstitial positions are also recognizable (Figure 2b).

The second phlogopite occurrence crops out on the western side of the Cannobino river (46° 06′ 15″ N – 08° 32′ 41″ E), where a pocket (8–10 cm wide) of phlogopite-bearing amphibole orthopyroxenite developed in sharp contact with the host peridotite (Figure 2c). A millimetre thick (up to 4 mm) phlogopite-bearing hornblendite vein starts from this pocket, crosscutting the host peridotite foliation at a

high angle. Rare orthopyroxene can be found along the vein. In this outcrop, another phlogopite-bearing pocket was recognized but was impossible to collect.

The sampled pocket exhibits a larger grain size than the vein and has the following modal composition: orthopyroxene (54%), phlogopite (38%), amphibole (7%), spinel (1%) and accessory granoblastic olivine. Orthopyroxene is euhedral to subhedral, often containing clinopyroxene exolution lamellae. Black spinel occurs in an interstitial position or as an inclusion within amphibole and phlogopite. The phlogopite occurs in large aggregates of flakes and rarely as an interstitial phase. Olivine is present in two different microtextural positions: as small anhedral crystals placed in contact by triple junctions, and/or as small rounded inclusions within orthopyroxene.

The host peridotite is a dunite with a foliated texture, containing small amounts of disseminated amphibole, phlogopite and rare orthopyroxene in interstitial positions as late phases of crystallization. Phlogopite crystals occur in the host peridotite up to 6.7 cm from the pocket. The rock foliation is marked by the elongation of black spinel and olivine crystals. Near the vein, the dunite is porphyroclastic. This texture is characterized by more elongated olivine porphyroclasts compared to the "normal" dunite, an increase in the spinel grain size, and the presence of small olivine neoblasts.

4. Analytical methods

Samples were collected from both the phlogopite-bearing band (samples FN43, FI9714 and FI9715, labelled as Band in figures and tables) and the phlogopite-bearing pocket (sample Amphlog, labelled as Pocket in figures and tables). The major-element composition of mineral phases was determined by electron microprobe according to the methodology reported by Rivalenti et al. [27].

Data were checked and corrected using cation mass balance with different O normalization for each phase (amphibole: 23 O p.f.u.; mica: 22 O p.f.u.; orthopyroxene: 6 O p.f.u.; olivine and spinel: 4 O p.f.u.). Data are reported in Table 1.

Trace-elements have been determined at the Centro Interdipartimentale Grandi Strumenti (C.I.G.S.) of the University of Modena and Reggio Emilia by means of a Thermo Fisher Scientific Mass Spectrometer coupled to a laser ablation New Wave UP 213. Data reduction was performed with Thermo Fisher Scientific PlasmaLab® software using NIST610, NIST612 and NIST614 as external standards. ^{44}Ca was used as internal standard for amphibole and ^{29}Si for phlogopite. Laser spot size was calibrated at 80 μm and laser beam fluency at 20 microJoule for cm^2. Data are reported in Table 2.

5. Mineral chemistry

5.1. Major-element composition

The olivine within the band-phlogopite-occurrence ("band" from now on) has Fo content between 0.85–0.87 (Fo = Mg# calculated as $[Mg^{2+}/(Mg^{2+}+Fe^{2+}_{tot})]$ molar ratio). Conversely, the olivine inclusions within the orthopyroxenite of the pocket-phlogopite-occurrence ("pocket" from now on) show Fo values between 0.87–0.89. The Fo content in the band is commonly below the average Fo composition (Fo = 0.87) reported by Siena & Coltorti [3] for the Amph-Pd unit, while the Fo content in the pocket is higher (Figure 3, Tables 1, 3 and 4).

Spinel in the pocket exhibits higher values of Al_2O_3 and MgO and lower Cr_2O_3 compared to the spinel in the band (Cr# calculated as $[Cr^{3+}/(Cr^{3+}+Al^{3+})]$, molar ratio, between 0.18–0.21 and 0.23–0.37 respectively, Tables 1 and 3). Pocket spinels are quite different from the average of spinel from the Amph-Pd unit (Siena & Coltorti [3]).

The band amphibole shows Al_2O_3 and MgO contents similar to the average of Siena & Coltorti [3], while FeO_{tot} and Cr_2O_3 abundances are lower and higher, respectively (Tables 1, 3 and 4). Amphibole, both from the band and the pocket, share similar major-element contents with the exception of Na_2O and K_2O. The pocket amphibole has lower Na_2O (2.03–2.27 wt.% and 1.90–3.39 wt.%, respectively) and higher K_2O contents (1.22–1.53 wt.% and 0.12–0.76 wt.% respectively, Tables 1 and 3) than the band amphibole. Amphibole from both the band and the pocket is dominantly pargasite and just one crystal from the band is edenite. The amphibole average composition reported by Siena & Coltorti [3] for the Amph-Pd unit falls inside the compositional range of the band amphibole. Amphibole from the pocket is in contrast quite distinct: i.e. lower SiO_2 and Na_2O and higher Al_2O_3 and K_2O (Tables 1, 3 and 4).

Similar to the amphibole composition, phlogopite from both the band and the pocket differs only in Na_2O and K_2O contents. Na_2O is higher in the band phlogopite compared to that in the pocket (1.08–2.07 wt.% and 0.82–1.15 wt.% respectively, Table 1). However, K_2O is higher in the pocket phlogopite than in the band phlogopite (8.75–9.89 wt.% and 6.00–8.23 wt.% respectively, Tables 1 and 3).

Orthopyroxene occurs only in the pocket and not in the band. The average major-element composition of orthopyroxene reported by Siena & Coltorti [3] in the Amph-Pd unit is similar to that of orthopyroxene in the pocket. They differ only in FeO content, which is higher in the pocket orthopyroxenes (7.84–8.64 wt.% and 7.48 wt.%, respectively; Tables 1, 3 and 4).

Table 1. Major-element composition of mineral phases as wt.%, a.p.f.u. Formulae and Mg# calculated as $Mg^{2+}/(Mg^{2+}+Fe^{2+}_{tot})$.

Sample							Pocket						
Phase							Opx						
Site	1	1	3	3	4	4	5	6	6	6	7	7	8
Analysis n.	5	6	9	10	12	13	16	17	18	19	20	21	23
Position	rim	core	core	rim	core	rim	core	core	rim	rim	core	rim	core
SiO_2	55.82	55.82	55.70	56.73	55.48	55.99	55.87	55.60	56.50	56.48	56.20	56.17	55.85
TiO_2	0.00	0.05	0.10	0.00	0.00	0.00	0.02	0.02	0.00	0.05	0.00	0.00	0.06
Al_2O_3	2.31	2.62	2.78	1.40	2.71	2.82	2.40	2.99	2.01	1.84	2.31	2.40	2.69
Cr_2O_3	0.09	0.14	0.15	0.11	0.24	0.23	0.27	0.27	0.00	0.20	0.22	0.16	0.26
FeO_T	8.38	8.32	8.37	8.29	8.55	8.33	8.51	8.34	8.60	8.64	7.99	8.28	8.39
MnO	0.25	0.21	0.17	0.15	0.25	0.19	0.18	0.15	0.00	0.26	0.27	0.20	0.31
NiO	0.03	0.05	0.00	0.00	0.09	0.03	0.01	0.00	0.00	0.00	0.09	0.01	0.08
MgO	32.35	32.31	32.26	33.04	31.94	32.33	32.30	32.22	32.84	32.71	32.71	32.70	32.21
CaO	0.31	0.41	0.49	0.29	0.38	0.50	0.41	0.42	0.32	0.28	0.35	0.29	0.51
Na_2O													
K_2O													
Total	99.54	99.93	100.02	100.01	99.64	100.42	99.97	100.01	100.27	100.46	100.14	100.21	100.36
a.p.f.u.													
Si	1.95	1.94	1.94	1.97	1.94	1.94	1.95	1.93	1.96	1.96	1.95	1.95	1.94
Ti	0.00	0.00	0.00	0.00	0.00	0.00	0.00	0.00	0.00	0.00	0.00	0.00	0.00
Al	0.10	0.11	0.11	0.06	0.11	0.12	0.10	0.12	0.08	0.08	0.09	0.10	0.11
Cr	0.00	0.00	0.00	0.00	0.01	0.01	0.01	0.01	0.00	0.01	0.01	0.00	0.01
Fe^{2+}	0.24	0.24	0.24	0.24	0.25	0.24	0.25	0.24	0.25	0.25	0.23	0.24	0.24
Fe^{3+}	0.00	0.00	0.00	0.00	0.00	0.00	0.00	0.00	0.00	0.00	0.00	0.00	0.00
Mn	0.01	0.01	0.01	0.00	0.01	0.01	0.01	0.00	0.00	0.01	0.01	0.01	0.01
Ni	0.00	0.00	0.00	0.00	0.00	0.00	0.00	0.00	0.00	0.00	0.00	0.00	0.00
Mg	1.69	1.68	1.67	1.71	1.67	1.67	1.68	1.67	1.70	1.69	1.69	1.69	1.67
Ca	0.01	0.02	0.02	0.01	0.01	0.02	0.02	0.02	0.01	0.01	0.01	0.01	0.02
Na													
K													
cations	4.00	4.00	4.00	4.00	4.00	4.00	4.00	4.00	4.00	4.00	4.00	4.00	4.00
Mg#	0.87	0.87	0.87	0.88	0.87	0.87	0.87	0.87	0.87	0.87	0.88	0.88	0.87

Sample	Pocket													
Phase	Opx													
Site	8	9	9	10	10	11	11	12	13	14	14	15	16	16
Analysis n.	24	25	26	29	30	31	32	34	36	39	42	43	45	46
Position	rim	core	rim	core	rim	core	rim	core	core	core	core	core	core	rim
SiO_2	55.92	55.79	56.05	55.61	56.19	56.00	55.87	55.68	56.00	55.74	55.57	56.08	55.99	55.76
TiO_2	0.00	0.05	0.00	0.00	0.00	0.00	0.03	0.00	0.00	0.01	0.12	0.03	0.00	0.03
Al_2O_3	2.62	2.75	2.32	2.83	2.01	2.46	2.67	2.67	2.91	2.78	2.65	2.33	2.43	2.61
Cr_2O_3	0.25	0.33	0.20	0.15	0.22	0.10	0.26	0.12	0.22	0.21	0.23	0.20	0.14	0.24
FeO_T	8.10	8.33	8.06	8.21	8.16	8.12	8.30	8.07	8.28	8.30	7.94	8.15	7.95	8.04
MnO	0.19	0.17	0.25	0.24	0.19	0.26	0.19	0.18	0.18	0.12	0.21	0.23	0.18	0.24
NiO	0.09	0.15	0.00	0.00	0.05	0.04	0.12	0.07	0.10	0.00	0.11	0.15	0.04	0.05
MgO	32.54	32.24	32.64	32.19	32.70	32.60	32.41	32.30	32.36	32.26	32.41	32.52	32.59	32.46
CaO	0.28	0.50	0.41	0.41	0.37	0.46	0.34	0.48	0.46	0.48	0.43	0.41	0.45	0.38
Na_2O														
K_2O														
Total	99.99	100.31	99.93	99.64	99.89	100.04	100.19	99.57	100.51	99.90	99.67	100.10	99.77	99.81
a.p.f.u.														
Si	1.94	1.94	1.95	1.94	1.96	1.95	1.94	1.94	1.94	1.94	1.94	1.95	1.95	1.94
Ti	0.00	0.00	0.00	0.00	0.00	0.00	0.00	0.00	0.00	0.00	0.00	0.00	0.00	0.00
Al	0.11	0.11	0.10	0.12	0.08	0.10	0.11	0.11	0.12	0.11	0.11	0.10	0.10	0.11
Cr	0.01	0.01	0.01	0.00	0.01	0.00	0.01	0.00	0.01	0.01	0.01	0.01	0.00	0.01
Fe^{2+}	0.24	0.24	0.23	0.24	0.24	0.23	0.24	0.24	0.24	0.24	0.23	0.24	0.23	0.23
Fe^{3+}	0.00	0.00	0.00	0.00	0.00	0.00	0.00	0.00	0.00	0.00	0.00	0.00	0.00	0.00
Mn	0.01	0.01	0.01	0.01	0.01	0.01	0.01	0.01	0.01	0.00	0.01	0.01	0.01	0.01
Ni	0.00	0.00	0.00	0.00	0.00	0.00	0.00	0.00	0.00	0.00	0.00	0.00	0.00	0.00
Mg	1.69	1.67	1.69	1.67	1.70	1.69	1.68	1.68	1.67	1.67	1.69	1.69	1.69	1.69
Ca	0.01	0.02	0.02	0.02	0.01	0.02	0.01	0.02	0.02	0.02	0.02	0.02	0.02	0.01
Na														
K														
cations	4.00	4.00	4.00	4.00	4.00	4.00	4.00	4.00	4.00	4.00	4.00	4.00	4.00	4.00
Mg#	0.88	0.87	0.88	0.87	0.88	0.88	0.87	0.88	0.87	0.87	0.88	0.88	0.88	0.88

Sample	Pocket						Pocket						
Phase	Opx						Ol						
Site	19	21	22	23	25	27	3	9	9	11	13	13	14
Analysis n.	52	58	59	62	68	72	11	27	28	33	37	38	40
Position	core	core	core	core	core	core	core	core	core	rim	core	rim	core
SiO_2	56.12	55.71	55.94	56.12	56.12	56.19	40.07	40.02	40.24	40.39	40.40	40.29	40.26
TiO_2	0.04	0.00	0.03	0.00	0.00	0.06	0.00	0.00	0.00	0.00	0.00	0.00	0.00
Al_2O_3	2.48	2.38	2.58	2.55	2.34	2.13	0.20	0.22	0.17	0.03	0.00	0.00	0.00
Cr_2O_3	0.11	0.16	0.21	0.22	0.13	0.22	0.00	0.00	0.00	0.00	0.05	0.05	0.00
FeOT	7.84	8.20	7.92	8.16	7.88	7.94	12.66	12.63	12.37	12.16	12.07	11.99	11.88
MnO	0.24	0.26	0.23	0.12	0.32	0.22	0.15	0.19	0.32	0.11	0.20	0.29	0.22
NiO	0.00	0.11	0.13	0.08	0.05	0.08	0.24	0.18	0.17	0.05	0.14	0.15	0.18
MgO	32.78	32.27	32.57	32.68	32.68	32.87	46.52	46.48	46.85	47.26	47.19	47.08	47.15
CaO	0.51	0.40	0.39	0.36	0.43	0.22	0.00	0.00	0.00	0.02	0.00	0.01	0.00
Na_2O													
K2O													
Total	100.12	99.49	100.00	100.29	99.95	99.93	99.84	99.72	100.12	100.02	100.05	99.86	99.69
a.p.f.u.													
Si	1.95	1.95	1.94	1.95	1.95	1.95	1.00	1.00	1.00	1.00	1.00	1.00	1.00
Ti	0.00	0.00	0.00	0.00	0.00	0.00	0.00	0.00	0.00	0.00	0.00	0.00	0.00
Al	0.10	0.10	0.11	0.10	0.10	0.09	0.01	0.01	0.00	0.00	0.00	0.00	0.00
Cr	0.00	0.00	0.01	0.01	0.00	0.01	0.00	0.00	0.00	0.00	0.00	0.00	0.00
Fe^{2+}	0.23	0.24	0.23	0.24	0.23	0.23	0.26	0.26	0.26	0.25	0.25	0.25	0.25
Fe^{3+}	0.00	0.00	0.00	0.00	0.00	0.00	0.00	0.00	0.00	0.00	0.00	0.00	0.00
Mn	0.01	0.01	0.01	0.00	0.01	0.01	0.00	0.00	0.01	0.00	0.00	0.01	0.00
Ni	0.00	0.00	0.00	0.00	0.00	0.00	0.00	0.00	0.00	0.00	0.00	0.00	0.00
Mg	1.69	1.68	1.69	1.69	1.69	1.70	1.73	1.73	1.73	1.74	1.74	1.74	1.75
Ca	0.02	0.01	0.01	0.01	0.02	0.01	0.00	0.00	0.00	0.00	0.00	0.00	0.00
Na													
K													
cations	4.00	4.00	4.00	4.00	4.00	4.00	3.00	3.00	3.00	3.00	3.00	3.00	3.00
Mg#	0.88	0.88	0.88	0.88	0.88	0.88	0.87	0.87	0.87	0.87	0.87	0.87	0.88

Sample	Pocket					Band							
Phase	Ol					Ol							
Site	14	15	19	19	24	2	2	5	5	8	8	4	5
Analysis n.	41	44	53	54	67	1	2	5	6	9	10	8	10
Position	core	core	core	rim	core	core	rim	core	rim	core	rim	core	core
SiO_2	40.53	40.25	40.09	40.39	40.47	40.22	39.92	39.94	40.14	40.06	39.93	40.35	40.08
TiO_2	0.00	0.00	0.02	0.00	0.00	0.00	0.00	0.07	0.18	0.04	0.00	0.08	0.00
Al_2O_3	0.04	0.00	0.05	0.06	0.07	0.00	0.00	0.00	0.00	0.00	0.00	0.00	0.00
Cr_2O_3	0.00	0.07	0.03	0.04	0.00	0.29	0.23	0.00	0.04	0.14	0.00	0.00	0.15
FeO_T	12.35	12.38	12.41	12.48	10.62	13.42	13.46	13.49	13.37	12.90	14.09	13.13	12.94
MnO	0.13	0.18	0.17	0.28	0.25	0.22	0.55	0.04	0.32	0.15	0.00	0.00	0.00
NiO	0.18	0.18	0.19	0.15	0.16	0.00	0.00	0.07	0.07	0.00	0.00	0.14	0.79
MgO	47.27	46.89	46.56	46.91	48.05	46.22	45.49	45.92	45.96	46.34	45.63	46.66	46.04
CaO	0.00	0.04	0.02	0.04	0.16	0.00	0.00	0.00	0.00	0.00	0.00	0.00	0.00
Na_2O													
K_2O													
Total	100.50	99.99	99.54	100.35	99.78	100.37	99.65	99.53	100.08	99.63	99.65	100.36	100.00
a.p.f.u.													
Si	1.00	1.00	1.00	1.00	1.00	1.00	1.00	1.00	1.00	1.00	1.00	1.00	1.00
Ti	0.00	0.00	0.00	0.00	0.00	0.00	0.00	0.00	0.00	0.00	0.00	0.00	0.00
Al	0.00	0.00	0.00	0.00	0.00	0.00	0.00	0.00	0.00	0.00	0.00	0.00	0.00
Cr	0.00	0.00	0.00	0.00	0.00	0.01	0.00	0.00	0.00	0.00	0.00	0.00	0.00
Fe^{2+}	0.25	0.26	0.26	0.26	0.22	0.28	0.28	0.28	0.28	0.27	0.30	0.27	0.27
Fe^{3+}	0.00	0.00	0.00	0.00	0.00	0.00	0.00	0.00	0.00	0.00	0.00	0.00	0.00
Mn	0.00	0.00	0.00	0.01	0.01	0.00	0.01	0.00	0.01	0.00	0.00	0.00	0.00
Ni	0.00	0.00	0.00	0.00	0.00	0.00	0.00	0.00	0.00	0.00	0.00	0.00	0.02
Mg	1.74	1.73	1.73	1.73	1.77	1.71	1.70	1.71	1.71	1.72	1.70	1.72	1.71
Ca	0.00	0.00	0.00	0.00	0.00	0.00	0.00	0.00	0.00	0.00	0.00	0.00	0.00
Na													
K													
cations	3.00	3.00	3.00	3.00	3.00	3.00	3.00	3.00	3.00	3.00	3.00	3.00	3.00
Mg#	0.87	0.87	0.87	0.87	0.89	0.86	0.86	0.86	0.86	0.86	0.85	0.86	0.86

Sample	Band													
Phase	Ol													
Site	5	7	8	8	11	11	11	11	11	11	14	14	15	15
Analysis n.	11	16	18	19	26	27	28	29	30	31	38	39	40	41
Position	rim	core	core	rim	core	core	core	core	core	core	core	rim	core	rim
SiO_2	40.34	40.18	40.10	39.67	40.15	40.41	40.44	40.14	40.18	40.23	40.08	40.33	39.95	40.17
TiO_2	b.d.l.	b.d.l.	b.d.l.	b.d.l.	0.01	b.d.l.	b.d.l.	0.31	b.d.l.	b.d.l.	0.06	0.35	0.10	0.46
Al_2O_3	b.d.l.	b.d.l.	b.d.l.	b.d.l.	b.d.l.	b.d.l.	b.d.l.	b.d.l.	b.d.l.	b.d.l.	b.d.l.	b.d.l.	b.d.l.	b.d.l.
Cr_2O_3	b.d.l.	0.24	0.30	b.d.l.	b.d.l.	0.24	0.02	0.04	b.d.l.	b.d.l.	0.07	b.d.l.	b.d.l.	b.d.l.
FeOT	13.13	13.04	13.39	14.48	13.30	12.41	12.44	12.01	12.72	13.02	12.54	13.54	13.16	12.48
MnO	0.21	b.d.l.	0.25	b.d.l.	0.38	0.03	0.07	0.23	b.d.l.	b.d.l.	0.53	0.11	0.16	0.51
NiO	0.20	b.d.l.	0.47	0.83	0.08	0.28	0.31	0.38	0.14	b.d.l.	0.66	b.d.l.	0.38	0.72
MgO	46.54	46.55	45.70	44.69	46.11	46.91	47.03	46.42	46.70	46.63	45.95	46.06	45.88	45.73
CaO	b.d.l.	b.d.l.	b.d.l.	b.d.l.	b.d.l.	b.d.l.	b.d.l.	b.d.l.	b.d.l.	b.d.l.	b.d.l.	b.d.l.	b.d.l.	b.d.l.
Na_2O														
K_2O														
Total	100.42	100.01	100.21	99.67	100.03	100.28	100.31	99.53	99.74	99.88	99.89	100.39	99.63	100.07
a.p.f.u.														
Si	1.00	1.00	1.00	1.00	1.00	1.00	1.00	1.00	1.00	1.00	1.00	1.00	1.00	1.00
Ti	0.00	0.00	0.00	0.00	0.00	0.00	0.00	0.01	0.00	0.00	0.00	0.01	0.00	0.01
Al	0.00	0.00	0.00	0.00	0.00	0.00	0.00	0.00	0.00	0.00	0.00	0.00	0.00	0.00
Cr	0.00	0.00	0.01	0.00	0.00	0.00	0.00	0.00	0.00	0.00	0.00	0.00	0.00	0.00
Fe^{2+}	0.27	0.27	0.28	0.30	0.28	0.26	0.26	0.25	0.26	0.27	0.26	0.28	0.28	0.26
Fe^{3+}	0.00	0.00	0.00	0.00	0.00	0.00	0.00	0.00	0.00	0.00	0.00	0.00	0.00	0.00
Mn	0.00	0.00	0.01	0.00	0.01	0.00	0.00	0.00	0.00	0.00	0.01	0.00	0.00	0.01
Ni	0.00	0.00	0.01	0.02	0.00	0.01	0.01	0.01	0.00	0.00	0.01	0.00	0.01	0.01
Mg	1.72	1.72	1.70	1.68	1.71	1.73	1.73	1.72	1.73	1.73	1.71	1.70	1.71	1.70
Ca	0.00	0.00	0.00	0.00	0.00	0.00	0.00	0.00	0.00	0.00	0.00	0.00	0.00	0.00
Na														
K														
cations	3.00	3.00	3.00	3.00	3.00	3.00	3.00	2.99	3.00	3.00	3.00	2.99	3.00	2.99
Mg#	0.86	0.86	0.86	0.85	0.86	0.87	0.87	0.87	0.87	0.86	0.87	0.86	0.86	0.87

Sample	Pocket				Band						Pocket	
Phase	Sp				Sp						Amph	
Site	7	23	24	24	7	7	12	13	15	9	5	5
Analysis n.	22	63	64	65	7	8	19	20	24	20	14	15
Position	core	core	core	rim	core	rim	core	core	core	core	core	rim
SiO_2											44.13	44.29
TiO_2	b.d.l.	0.01	b.d.l.	b.d.l.	b.d.l.	b.d.l.	b.d.l.	b.d.l.	b.d.l.	b.d.l.	0.53	0.43
Al_2O_3	47.74	45.86	49.39	48.82	45.66	46.90	36.20	39.41	43.39	39.47	13.93	13.57
Cr_2O_3	17.83	17.87	16.59	17.45	22.27	21.29	32.63	29.31	24.69	30.12	0.96	0.74
FeO_T	17.29	19.53	17.93	18.50	18.74	16.69	18.95	18.40	19.81	16.50	4.90	5.43
MnO	b.d.l.	0.06	b.d.l.	b.d.l.	b.d.l.	b.d.l.	b.d.l.	b.d.l.	b.d.l.	b.d.l.	0.04	0.01
NiO	0.22	0.14	0.32	0.27	b.d.l.	b.d.l.	b.d.l.	b.d.l.	b.d.l.	b.d.l.	0.16	b.d.l.
MgO	16.10	15.83	16.11	15.72	13.45	14.83	12.33	13.04	12.59	14.33	16.75	16.63
CaO	b.d.l.	0.13	b.d.l.	b.d.l.	b.d.l.	b.d.l.	b.d.l.	b.d.l.	b.d.l.	b.d.l.	12.62	12.82
Na_2O											2.12	2.03
K_2O											1.53	1.53
Total	99.18	99.43	100.34	100.76	100.12	99.71	100.11	100.16	100.48	100.42	97.67	97.48
a.p.f.u.												
Si											6.32	6.36
Ti	0.00	0.00	0.00	0.00	0.00	0.00	0.00	0.00	0.00	0.00	0.06	0.05
Al	1.55	1.50	1.58	1.56	1.51	1.53	1.25	1.33	1.45	1.32	2.35	2.30
Cr	0.39	0.39	0.36	0.37	0.49	0.47	0.75	0.67	0.55	0.68	0.11	0.08
Fe^{2+}	0.33	0.34	0.34	0.36	0.44	0.39	0.46	0.44	0.47	0.39	0.59	0.65
Fe^{3+}	0.06	0.11	0.06	0.06	0.00	0.00	0.00	0.00	0.00	0.00	0.00	0.00
Mn	0.00	0.00	0.00	0.00	0.00	0.00	0.00	0.00	0.00	0.00	0.00	0.00
Ni	0.00	0.00	0.01	0.01	0.00	0.00	0.00	0.00	0.00	0.00	0.02	0.00
Mg	0.66	0.65	0.65	0.64	0.56	0.61	0.54	0.56	0.53	0.61	3.57	3.56
Ca	0.00	0.00	0.00	0.00	0.00	0.00	0.00	0.00	0.00	0.00	1.94	1.97
Na											0.59	0.57
K											0.28	0.28
cations	3.00	3.00	3.00	3.00	3.00	3.00	3.00	3.00	3.00	3.00	15.83	15.82
Mg#	0.62	0.59	0.62	0.60	0.56	0.61	0.54	0.56	0.53	0.61	0.86	0.85

Sample	Pocket								Band				
Phase	Amph								Amph				
Site	23	23	26	26	9	9	10	10	11	11	14	14	18
Analysis n.	60	61	70	71	11	12	13	14	15	16	21	22	28
Position	core	rim	core	rim	core	rim	core	rim	core	rim	core	rim	core
SiO_2	43.91	43.54	44.18	43.98	45.34	42.90	45.39	45.76	46.10	42.29	45.23	41.84	44.70
TiO_2	0.37	0.33	0.35	0.37	0.11	1.21	0.35	0.75	0.69	0.43	0.16	0.36	1.03
Al_2O_3	13.64	13.52	14.07	13.57	13.22	14.08	13.51	13.48	11.90	14.25	12.05	13.78	13.16
Cr_2O_3	0.92	0.97	0.94	0.94	1.34	1.69	1.47	0.47	0.83	1.32	0.98	1.56	1.25
FeOT	4.78	4.87	4.82	4.86	4.76	5.42	4.89	5.16	5.01	5.89	5.07	5.30	5.41
MnO	0.06	0.15	0.09	0.05	b.d.l.	b.d.l.	b.d.l.	b.d.l.	0.01	0.17	0.15	0.13	b.d.l.
NiO	0.18	0.11	0.13	0.09	b.d.l.	0.32	b.d.l.	b.d.l.	b.d.l.	0.08	b.d.l.	b.d.l.	b.d.l.
MgO	16.53	16.59	16.60	16.86	15.92	16.69	16.77	17.20	17.28	16.25	18.49	18.22	17.30
CaO	12.48	12.44	12.66	12.52	11.36	11.69	11.22	11.48	11.29	11.54	12.48	11.36	11.09
Na_2O	2.25	2.27	2.21	2.22	3.97	2.92	3.58	3.04	3.47	3.72	3.23	3.76	3.62
K_2O	1.31	1.38	1.37	1.22	0.65	0.39	0.39	0.48	0.76	0.27	0.12	0.39	0.30
Total	96.43	96.17	97.42	96.68	96.67	97.31	97.57	97.82	97.34	96.21	97.96	96.70	97.86
a.p.f.u.													
Si	6.36	6.34	6.34	6.35	6.52	6.18	6.45	6.48	6.58	6.18	6.44	6.08	6.36
Ti	0.04	0.04	0.04	0.04	0.01	0.13	0.04	0.08	0.07	0.05	0.02	0.04	0.11
Al	2.33	2.32	2.38	2.31	2.24	2.39	2.26	2.25	2.00	2.45	2.02	2.36	2.21
Cr	0.11	0.11	0.11	0.11	0.15	0.19	0.17	0.05	0.09	0.15	0.11	0.18	0.14
Fe^{2+}	0.58	0.59	0.58	0.59	0.57	0.65	0.58	0.61	0.60	0.72	0.60	0.64	0.64
Fe^{3+}	0.00	0.00	0.00	0.00	0.00	0.00	0.00	0.00	0.00	0.00	0.00	0.00	0.00
Mn	0.01	0.02	0.01	0.01	0.00	0.00	0.00	0.00	0.00	0.02	0.02	0.02	0.00
Ni	0.02	0.01	0.01	0.01	0.00	0.04	0.00	0.00	0.00	0.01	0.00	0.00	0.00
Mg	3.57	3.60	3.55	3.63	3.41	3.58	3.55	3.63	3.67	3.53	3.92	3.95	3.67
Ca	1.94	1.94	1.95	1.94	1.75	1.80	1.71	1.74	1.73	1.81	1.90	1.77	1.69
Na	0.63	0.64	0.61	0.62	1.11	0.82	0.99	0.83	0.96	1.05	0.89	1.06	1.00
K	0.24	0.26	0.25	0.22	0.12	0.07	0.07	0.09	0.14	0.05	0.02	0.07	0.05
cations	15.82	15.86	15.82	15.82	15.88	15.85	15.82	15.75	15.85	16.02	15.94	16.17	15.88
Mg#	0.86	0.86	0.86	0.86	0.86	0.85	0.86	0.86	0.86	0.83	0.87	0.86	0.85

Sample														
Phase	Band Amph													
Site	18	2	2	4	4	6	6	7	7	11	11	12	12	14
Analysis n.	29	5	6	7	9	13	14	15	17	24	25	32	33	37
Position	rim	rim	core	core	rim	core	rim	core	rim	core	rim	core	rim	core
SiO_2	45.31	44.75	43.80	44.87	42.77	43.47	45.22	43.85	45.02	43.18	43.52	45.00	43.96	42.85
TiO_2	0.77	0.70	0.97	0.42	0.16	0.73	0.11	0.74	0.58	1.15	0.72	0.15	0.58	0.50
Al_2O_3	13.09	13.33	13.58	13.76	13.46	13.34	12.84	12.72	12.89	13.52	14.05	13.12	12.94	13.86
Cr_2O_3	0.99	1.69	1.14	b.d.l.	0.71	1.29	1.03	0.68	1.10	1.15	0.83	1.21	0.85	0.70
FeO_T	5.76	5.13	5.31	5.54	6.31	6.06	6.71	6.54	4.65	5.70	5.59	7.07	6.25	6.77
MnO	b.d.l.	0.13	0.06	0.25	0.42	b.d.l.	b.d.l.	b.d.l.	b.d.l.	b.d.l.	0.18	0.22	b.d.l.	b.d.l.
NiO	b.d.l.	0.12	b.d.l.	b.d.l.	b.d.l.	0.43	0.11	b.d.l.	0.09	0.23	b.d.l.	b.d.l.	b.d.l.	0.12
MgO	15.57	16.51	16.51	15.84	20.56	16.65	16.87	17.08	16.63	17.13	16.29	16.07	16.25	17.52
CaO	12.49	12.81	12.33	12.81	10.33	11.92	12.33	11.52	12.79	12.05	12.11	12.35	13.14	12.26
Na_2O	2.88	2.37	3.47	2.71	2.64	3.34	1.90	3.99	2.71	2.81	2.90	2.51	2.84	2.79
K_2O	0.62	0.29	0.16	0.69	0.58	0.56	0.53	0.65	0.49	0.49	0.43	0.26	0.55	0.43
Total	97.48	97.83	97.33	96.89	97.94	97.79	97.65	97.77	96.95	97.41	96.62	97.96	97.36	97.80
a.p.f.u.														
Si	6.49	6.38	6.29	6.45	6.12	6.26	6.47	6.32	6.46	6.22	6.29	6.44	6.35	6.17
Ti	0.08	0.08	0.10	0.05	0.02	0.08	0.01	0.08	0.06	0.12	0.08	0.02	0.06	0.05
Al	2.21	2.24	2.30	2.33	2.27	2.26	2.17	2.16	2.18	2.29	2.39	2.21	2.20	2.35
Cr	0.11	0.19	0.13	0.00	0.08	0.15	0.12	0.08	0.12	0.13	0.09	0.14	0.10	0.08
Fe^{2+}	0.69	0.61	0.64	0.67	0.76	0.73	0.80	0.79	0.56	0.69	0.68	0.85	0.75	0.82
Fe^{3+}	0.00	0.00	0.00	0.00	0.00	0.00	0.00	0.00	0.00	0.00	0.00	0.00	0.00	0.00
Mn	0.00	0.02	0.01	0.03	0.05	0.00	0.00	0.00	0.00	0.00	0.02	0.03	0.00	0.00
Ni	0.00	0.01	0.00	0.00	0.00	0.05	0.01	0.00	0.01	0.03	0.00	0.00	0.00	0.01
Mg	3.32	3.50	3.53	3.39	4.38	3.57	3.59	3.66	3.55	3.67	3.51	3.42	3.49	3.76
Ca	1.92	1.96	1.90	1.97	1.58	1.84	1.89	1.78	1.97	1.86	1.88	1.89	2.03	1.89
Na	0.80	0.65	0.97	0.76	0.73	0.93	0.53	1.11	0.75	0.78	0.81	0.70	0.80	0.78
K	0.11	0.05	0.03	0.13	0.11	0.10	0.10	0.12	0.09	0.09	0.08	0.05	0.10	0.08
cations	15.73	15.69	15.89	15.78	16.10	15.97	15.69	16.10	15.75	15.88	15.83	15.74	15.89	15.99
Mg#	0.83	0.85	0.85	0.84	0.85	0.83	0.82	0.82	0.86	0.84	0.84	0.80	0.82	0.82

Sample	Pocket													
Phase	Phl													
Site	1	1	1	1	2	2	12	18	18	19	19	20	20	25
Analysis n.	1	2	3	4	7	8	35	48	49	50	51	56	57	69
Position	core	rim	core	rim	core	rim	core	core	rim	core	rim	core	rim	core
SiO_2	39.49	39.19	39.21	39.12	39.34	39.06	39.23	39.36	39.17	39.66	39.63	40.18	39.73	39.54
TiO_2	0.79	0.75	0.90	0.91	0.86	0.95	0.90	0.88	0.82	0.97	0.91	0.90	0.95	0.90
Al_2O_3	16.82	17.08	16.72	16.69	16.77	16.42	16.29	16.58	16.43	16.43	16.71	16.54	16.54	16.42
Cr_2O_3	0.39	0.48	0.43	0.41	0.41	0.46	0.68	0.42	0.41	0.43	0.43	0.53	0.59	0.55
FeO_T	4.34	4.43	4.01	4.24	4.27	4.38	4.07	3.67	3.86	3.88	4.00	3.95	3.69	4.00
MnO	0.02	b.d.l.	0.04	0.01	b.d.l.	0.04	0.05	0.09	0.09	0.02	0.02	0.05	0.09	0.06
NiO	b.d.l.	b.d.l.	b.d.l.	b.d.l.	b.d.l.	b.d.l.	b.d.l.	b.d.l.	b.d.l.	b.d.l.	b.d.l.	b.d.l.	b.d.l.	b.d.l.
MgO	22.16	23.13	22.60	22.71	21.88	22.66	22.13	22.05	22.77	22.56	22.31	22.50	22.91	22.67
CaO	b.d.l.	b.d.l.	b.d.l.	0.07	b.d.l.	0.02	0.12	0.19	0.24	0.23	0.10	0.22	0.16	0.18
Na_2O	0.96	0.82	0.90	0.87	0.82	0.91	0.88	0.89	0.97	0.94	0.91	0.96	0.91	0.94
K_2O	9.75	9.01	9.57	9.11	9.65	9.84	9.51	9.48	9.40	9.50	9.66	9.50	8.91	9.89
Total	94.72	94.89	94.38	94.14	94.00	94.74	93.86	93.61	94.16	94.62	94.68	95.33	94.48	95.15
a.p.f.u.														
Si	5.64	5.56	5.61	5.60	5.65	5.59	5.65	5.66	5.61	5.65	5.65	5.68	5.64	5.62
Ti	0.08	0.08	0.10	0.10	0.09	0.10	0.10	0.10	0.09	0.10	0.10	0.10	0.10	0.10
Al	2.83	2.86	2.82	2.82	2.84	2.77	2.76	2.81	2.78	2.76	2.81	2.76	2.77	2.75
Cr	0.04	0.05	0.05	0.05	0.05	0.05	0.08	0.05	0.05	0.05	0.05	0.06	0.07	0.06
Fe^{2+}	0.52	0.53	0.48	0.51	0.51	0.52	0.49	0.44	0.46	0.46	0.48	0.47	0.44	0.48
Fe^{3+}	0.00	0.00	0.00	0.00	0.00	0.00	0.00	0.00	0.00	0.00	0.00	0.00	0.00	0.00
Mn	0.00	0.00	0.00	0.00	0.00	0.00	0.01	0.01	0.01	0.00	0.00	0.01	0.01	0.01
Ni	0.00	0.00	0.00	0.00	0.00	0.00	0.00	0.00	0.00	0.00	0.00	0.00	0.00	0.00
Mg	4.71	4.89	4.81	4.84	4.68	4.83	4.74	4.72	4.86	4.79	4.73	4.74	4.85	4.80
Ca	0.00	0.00	0.00	0.01	0.00	0.00	0.02	0.03	0.04	0.04	0.02	0.03	0.02	0.03
Na	0.27	0.23	0.25	0.24	0.23	0.25	0.25	0.25	0.27	0.26	0.25	0.26	0.25	0.26
K	1.78	1.63	1.75	1.66	1.77	1.80	1.75	1.74	1.72	1.73	1.76	1.71	1.61	1.79
cations	15.86	15.83	15.86	15.82	15.81	15.92	15.83	15.81	15.88	15.84	15.83	15.81	15.77	15.90
Mg#	0.90	0.90	0.91	0.91	0.90	0.90	0.91	0.91	0.91	0.91	0.91	0.91	0.92	0.91

Sample	Pocket							Band					
Phase	Phl							Phl					
Site	27	24	3	3	12	12	14	16	17	17	2	6	11
Analysis n.	74	66	3	4	17	18	23	25	26	27	4	12	23
Position	core	core	core	rim	core	rim	core	core	core	rim	core	core	core
SiO_2	39.48	38.13	39.58	38.72	39.77	39.34	38.21	39.38	39.95	38.11	39.14	39.08	38.00
TiO_2	0.98	0.74	0.73	1.16	0.84	1.10	1.09	1.07	0.66	0.86	0.52	0.65	0.82
Al_2O_3	16.73	16.73	16.61	15.78	16.21	15.70	17.06	16.06	16.26	15.54	17.17	17.43	16.38
Cr_2O_3	0.46	1.66	0.65	1.04	0.73	0.47	0.96	0.95	0.89	1.26	0.49	0.63	0.60
FeO_T	3.73	4.02	3.47	4.48	3.91	4.44	3.85	4.29	3.98	4.71	4.32	3.65	4.28
MnO	0.07	0.06	b.d.l.	b.d.l.	0.23	b.d.l.	b.d.l.	0.25	b.d.l.	b.d.l.	0.12	0.37	b.d.l.
NiO	b.d.l.	b.d.l.	b.d.l.	b.d.l.	b.d.l.	b.d.l.	b.d.l.	b.d.l.	b.d.l.	b.d.l.	b.d.l.	b.d.l.	b.d.l.
MgO	22.49	22.85	24.44	23.26	23.73	24.62	23.10	23.79	22.70	23.75	25.81	23.73	25.76
CaO	0.22	0.20	b.d.l.	b.d.l.	b.d.l.	b.d.l.	b.d.l.	b.d.l.	b.d.l.	b.d.l.	0.18	0.13	b.d.l.
Na_2O	1.15	1.03	1.96	2.07	1.16	1.34	2.02	1.60	1.80	1.95	1.08	2.06	1.47
K_2O	9.08	8.75	7.47	7.38	8.11	7.53	7.76	7.39	8.23	7.78	6.00	6.42	7.02
Total	94.39	94.17	94.91	93.89	94.69	94.54	94.05	94.78	94.47	93.96	94.83	94.15	94.33
a.p.f.u.													
Si	5.63	5.48	5.57	5.55	5.63	5.58	5.46	5.58	5.68	5.49	5.48	5.52	5.40
Ti	0.11	0.08	0.08	0.13	0.09	0.12	0.12	0.11	0.07	0.09	0.05	0.07	0.09
Al	2.81	2.83	2.75	2.67	2.70	2.62	2.87	2.68	2.72	2.64	2.83	2.90	2.74
Cr	0.05	0.19	0.07	0.12	0.08	0.05	0.11	0.11	0.10	0.14	0.05	0.07	0.07
Fe^{2+}	0.44	0.48	0.41	0.54	0.46	0.53	0.46	0.51	0.47	0.57	0.51	0.43	0.51
Fe^{3+}	0.00	0.00	0.00	0.00	0.00	0.00	0.00	0.00	0.00	0.00	0.00	0.00	0.00
Mn	0.01	0.01	0.00	0.00	0.03	0.00	0.00	0.03	0.00	0.00	0.01	0.04	0.00
Ni	0.00	0.00	0.00	0.00	0.00	0.00	0.00	0.00	0.00	0.00	0.00	0.00	0.00
Mg	4.77	4.89	5.12	4.97	5.00	5.20	4.92	5.02	4.80	5.10	5.38	5.00	5.45
Ca	0.03	0.03	0.00	0.00	0.00	0.00	0.00	0.00	0.00	0.00	0.03	0.02	0.00
Na	0.32	0.29	0.53	0.58	0.32	0.37	0.56	0.44	0.50	0.54	0.29	0.56	0.41
K	1.65	1.60	1.34	1.35	1.46	1.36	1.42	1.33	1.49	1.43	1.07	1.16	1.27
cations	15.82	15.88	15.88	15.89	15.78	15.83	15.92	15.80	15.84	16.01	15.71	15.78	15.94
Mg#	0.91	0.91	0.93	0.90	0.92	0.91	0.91	0.91	0.91	0.90	0.91	0.92	0.91

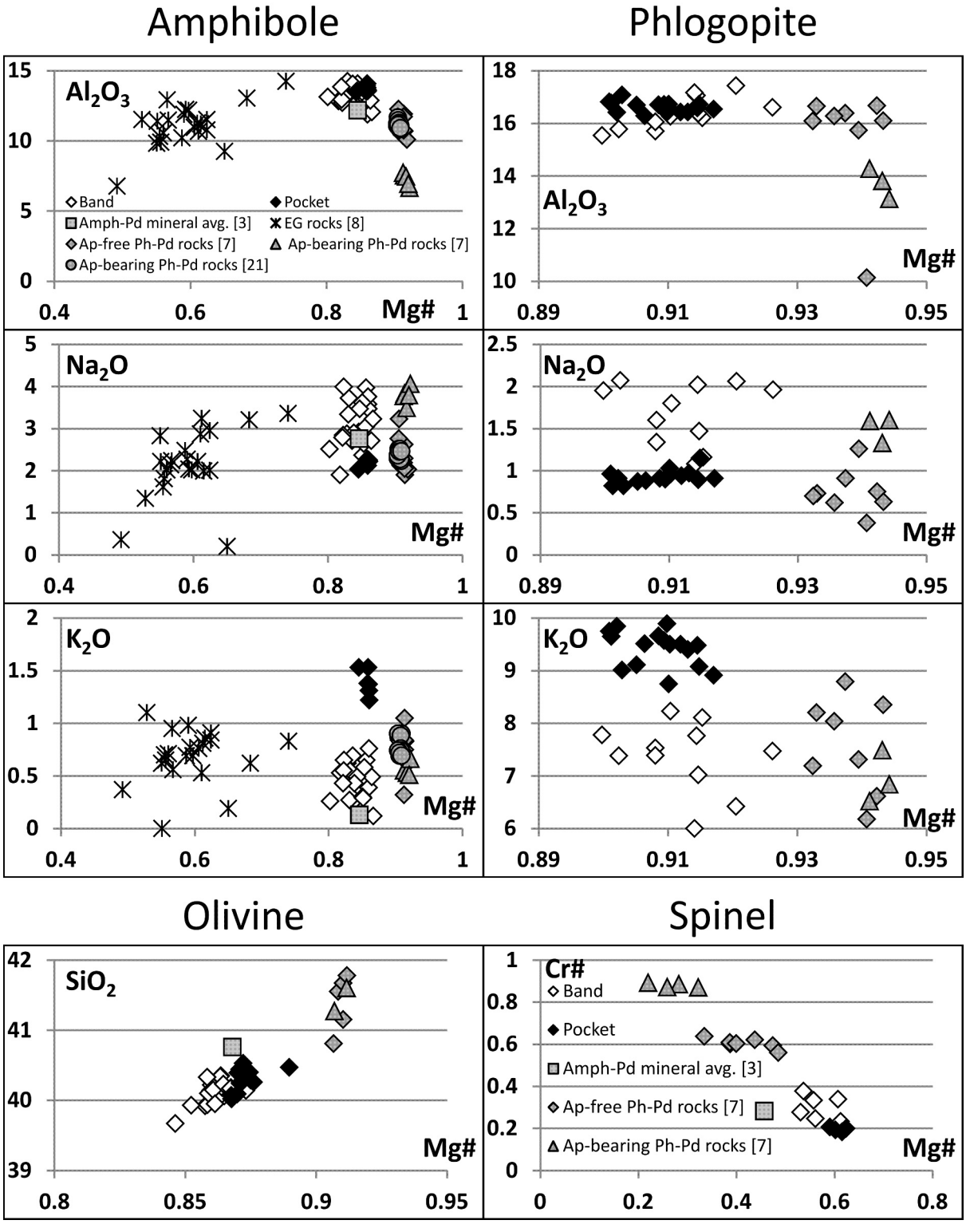

Figure 3. Major-element contents of phases in pocket, band and literature data. Plotted literature data are: Amph-Pd average mineral compositions from Siena & Coltorti [3], Ph-Pd mineral compositions from Zanetti et al. [7] and mineral composition of EG rocks from Zanetti et al. [8].

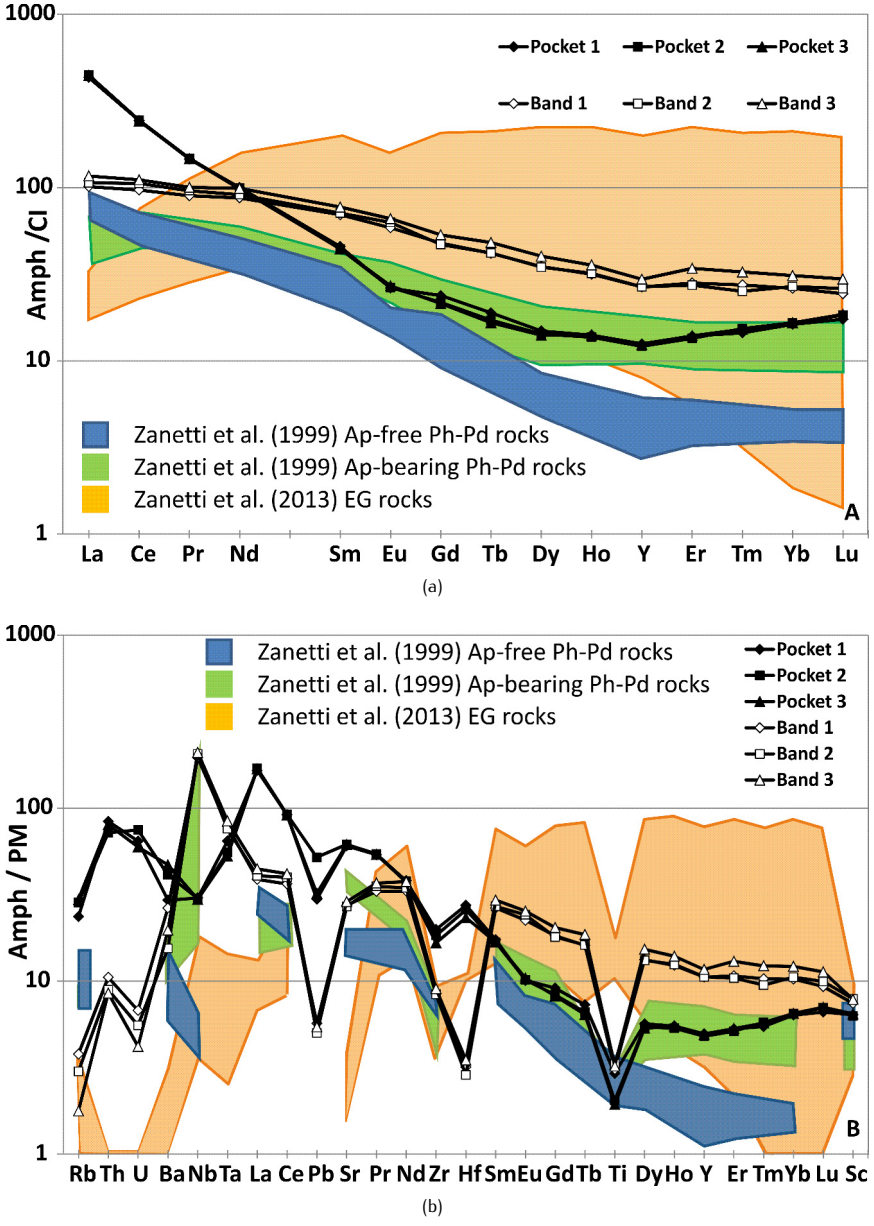

Figure 4. a) CI chondrite-normalized REE patterns of amphibole from the phlogopite-bearing samples from Amph-Pd and literature data. CI chondrite values are from Anders & Ebihara [28]. b) Primitive mantle (PM)-normalized trace-element patterns of amphibole from the phlogopite-bearing samples from Amph-Pd and literature data. Primitive mantle values are from Hofmann [29].

5.2. Trace-element composition

5.2.1. Amphibole

The amphiboles from the band and the pocket display different REE patterns (normalized to the CI chondrite values reported by Anders & Ebihara [28]) (Figure 4a, Tables 2 and 3). The pocket amphiboles show extremely LREE-enriched patterns (La_N = 430–440; La_N/Yb_N = 26.53–26.80), which are linearly fractionated in the LREE-MREE region (La_N/Sm_N = 9.44–10.07, La_N/Dy_N = 28.95–31.37), with an inversion of the slope (from negative to positive) in the HREE region (Figure 4a, Tables 2 and 3). The REE patterns of the band amphibole (Figure 4a, Tables 2 and 3) are still LREE enriched compared to the MREE and HREE (Figure 4a, Tables 2 and 3), but they show a lower fractionation (La_N/Sm_N = 1.45–1.51; La_N/Yb_N = 3.75–3.95),

Table 2. Trace-element compositions of amphiboles and phlogopites in ppm.

Sample	Pocket			Band						Pocket			Band			
Phase	Amph			Amph						Phl			Phl			
Site	5	23	26	10	10	14	14	18	18	1	2	18	12	12	17	17
Analysis n.	14	60	70	13	14	21	22	28	29	1	7	48	17	18	26	27
Position	core	core	core	core	rim	core	rim	core	rim	core	core	core	core	rim	core	rim
ppm																
Sc	95	94	96	105	117	124	111	110	123	10	9.7	10	10	10	11	10
Ti	2030	2062	2063	3265	3436	3757	3455	3294	3720	3235	3193	3187	4986	4856	4299	4136
V	139	130	127	44	91	122	73	100	113	114	116	130			42	40
Cr	6413	6519	6511	9100	8743	8739	8723	7910	8589	2975	3021	3137			4136	4088
Co	42	42	43	31	33	34	33	30	31	60	59	60	35	41	38	37
Ni	306	296	302	363	381	405	379	356	393	575	569	577	742	745	674	635
Rb	13	15	16	2.20	1.86	0.640	2.58	0.915	0.988	862	832	829	240	231	71	66
Sr	1099	1123	1120	494	505	505	478	494	553	231	220	211	220	213	285	264
Y	20	19	19	40	43	44	40	43	49	0.018	0.011	0.013	0.042	0.204	0.073	0.110
Zr	193	179	162	80	85	84	79	84	92	12	12	11	2.29	2.29	2.65	2.94
Nb	19	19	18	118	124	133	121	122	138	15	14	15	72	71	76	70
Cs	0.029	0.167	0.089	0.018	0.074		0.278		0.033	12	10	14	6.3	6.4	1.29	1.28
Ba	178	249	284	173	148	81	106	116	122	5379	4842	5502	6763	6702	5172	4484
La	101	104	103	23	25	26	23	26	29	0.025	0.017	0.006	0.021	0.255	0.082	0.098
Ce	147	147	146	56	60	68	60	63	71	0.005	0.006	0.006	0.029	0.229	0.115	0.154
Pr	13	13	13	7.9	8.1	9.1	8.0	8.5	9.3	0.003			0.003	0.027	0.012	0.026
Nd	45	45	44	39	40	43	39	42	47	0.005	0.003		0.003	0.071	0.031	0.050
Sm	6.7	6.5	6.5	10	10	11	10	11	12	0.003	0.003	0.006	0.004	0.041	0.017	0.031
Eu	1.47	1.48	1.52	3.3	3.3	3.8	3.3	3.5	3.9	0.028	0.022	0.021	0.023	0.022	0.038	0.024
Gd	4.7	4.3	4.2	9.2	9.6	9.7	8.8	9.7	11	0.009	0.003	0.005	0.012	0.011	0.014	0.020
Tb	0.687	0.623	0.602	1.49	1.54	1.65	1.39	1.66	1.83				0.002	0.012	0.002	0.006
Dy	3.6	3.5	3.4	8.4	8.6	8.9	7.9	9.2	10	0.002	0.002	0.002		0.042	0.002	0.023
Ho	0.783	0.761	0.781	1.67	1.85	1.87	1.69	1.87	2.09				0.004	0.030		0.003
Er	2.21	2.14	2.22	4.3	4.7	4.5	4.1	5.1	5.7		0.002		0.005	0.040	0.005	0.008
Tm	0.351	0.372	0.368	0.618	0.710	0.668	0.552	0.750	0.827	0.001	0.002	0.001	0.003	0.002	0.003	0.007
Yb	2.64	2.69	2.70	4.0	4.5	4.6	4.1	4.7	5.4	0.001	0.001	0.000	0.004	0.042	0.009	0.017
Lu	0.422	0.447	0.450	0.552	0.633	0.692	0.577	0.663	0.779	0.001	0.001	0.001		0.006	0.001	0.001
Hf	7.3	6.9	6.2	0.848	0.857	0.833	0.702	0.905	0.965	0.347	0.334	0.315	0.013	0.011	0.039	0.034
Ta	2.27	1.95	1.86	2.78	2.73	2.82	2.51	2.80	3.1	1.45	1.44	1.48	1.52	1.57	1.64	1.52
Pb	5.2	9.1	5.6	0.954	1.04	0.906	0.849	0.937	0.966	5.2	5.1	4.6	1.85	2.24	3.0	2.48
Th	6.8	5.9	6.5	0.795	0.917	0.679	0.771	0.679	0.706	0.001		0.001	0.002	0.003	0.004	0.017
U	1.31	1.52	1.21	0.119	0.156	0.105	0.12	0.087	0.084	0.016	0.026	0.015	0.003	0.005	0.001	0.010

Table 3. Minimum (Min.), maximum (Max.), average (Avg.) and standard deviation (std. dev.) of mineral phases from pocket and band.

Sample	Pocket				Pocket				Band				Pocket				Band			
Phase	Opx				Ol				Ol				Sp				Sp			
Type	Min.	Max.	Avg.	std. dev.	Min.	Max.	Avg.	std. dev.	Min.	Max.	Avg.	std. dev.	Min.	Max.	Avg.	std. dev.	Min.	Max.	Avg.	std. dev.
SiO_2	55.48	56.73	55.96	0.28	40.02	40.53	40.28	0.16	39.67	40.44	40.14	0.18								
TiO_2		0.12	0.02	0.03	0.00	0.02	0.00	0.01	0.00	0.46	0.08	0.13	0.00	0.01	0.00	0.01	0.00	0.00	0.00	0.00
Al_2O_3	1.40	2.99	2.48	0.33									45.86	49.39	47.95	1.55	36.20	46.90	41.84	4.15
Cr_2O_3		0.33	0.19	0.07	0.00	0.07	0.02	0.03	0.00	0.30	0.08	0.11	16.59	17.87	17.44	0.59	21.29	32.63	26.72	4.62
FeO_T	7.84	8.64	8.21	0.21	10.62	12.66	12.17	0.54	12.01	14.48	13.11	0.56	17.29	19.53	18.31	0.95	16.50	19.81	18.18	1.32
MnO		0.32	0.21	0.06	0.11	0.32	0.21	0.07	0.00	0.55	0.17	0.19	0.00	0.06	0.02	0.03	0.00	0.00	0.00	0.00
NiO		0.15	0.05	0.05	0.05	0.24	0.16	0.04	0.00	0.83	0.25	0.28	0.14	0.32	0.24	0.08	0.00	0.00	0.00	0.00
MgO	31.94	33.04	32.48	0.24	46.48	48.05	47.02	0.43	44.69	47.03	46.14	0.53	15.72	16.11	15.94	0.20	12.33	14.83	13.43	0.98
CaO	0.22	0.51	0.40	0.08									0.00	0.13	0.03	0.07	0.00	0.00	0.00	0.00

Sample	Pocket				Band				Pocket				Band			
Phase	Amph				Amph				Phl				Phl			
Type	Min.	Max.	Avg.	std. dev.	Min.	Max.	Avg.	std. dev.	Min.	Max.	Avg.	std. dev.	Min.	Max.	Avg.	std. dev.
SiO_2	43.54	44.29	44.01	0.27	41.84	46.10	44.22	1.20	38.13	40.18	39.35	0.43	38.00	39.95	39.03	0.68
TiO_2	0.33	0.53	0.40	0.07	0.11	1.21	0.58	0.33	0.74	0.98	0.88	0.07	0.52	1.16	0.86	0.22
Al_2O_3	13.52	14.07	13.72	0.23	11.90	14.25	13.30	0.59	16.29	17.08	16.62	0.20	15.54	17.43	16.38	0.63
Cr_2O_3	0.74	0.97	0.91	0.09	0.00	1.69	1.06	0.40	0.39	1.66	0.55	0.31	0.47	1.26	0.79	0.25
FeO_T	4.78	5.43	4.94	0.24	4.65	7.07	5.67	0.68	3.67	4.43	4.03	0.24	3.47	4.71	4.13	0.38
MnO	0.01	0.15	0.07	0.05	0.00	0.42	0.07	0.11	0.00	0.09	0.04	0.03	0.00	0.37	0.09	0.13
NiO	0.00	0.18	0.11	0.06	0.00	0.43	0.07	0.12	0.00	0.00	0.00	0.00	0.00	0.00	0.00	0.00
MgO	16.53	16.86	16.66	0.12	15.57	20.56	16.94	1.06	21.88	23.13	22.52	0.34	22.70	25.81	24.06	1.01
CaO	12.44	12.82	12.59	0.14	10.33	13.14	11.95	0.69	0.00	0.24	0.12	0.09	0.00	0.18	0.03	0.06
Na_2O	2.03	2.27	2.18	0.09	1.90	3.99	3.09	0.54	0.82	1.15	0.93	0.08	1.08	2.07	1.68	0.37
K_2O	1.22	1.53	1.39	0.12	0.12	0.76	0.46	0.17	8.75	9.89	9.41	0.34	6.00	8.23	7.37	0.67
$(La/Yb)_N$	26.53	26.80	26.62	0.15	3.75	3.95	3.86	0.10	13.99	17.66	15.82	2.59	3.92	5.15	4.53	0.87
$(La/Sm)_N$	9.44	10.07	9.82	0.34	1.45	1.51	1.49	0.03	0.63	5.27	3.15	2.35	2.50	3.59	3.05	0.77
$(Sm/Yb)_N$	2.66	2.81	2.71	0.09	2.48	2.66	2.60	0.10	2.65	4.97	3.81	1.64	1.09	2.05	1.57	0.68
$(Th/U)_N$	0.96	1.35	1.20	0.21	1.55	2.03	1.73	0.26	0.01	0.02	0.01	0.01	0.16	0.48	0.32	0.23
$(Zr/Hf)_N$	0.71	0.73	0.72	0.01	2.59	2.93	2.73	0.18	0.92	1.01	0.97	0.04	2.11	5.26	3.68	2.23

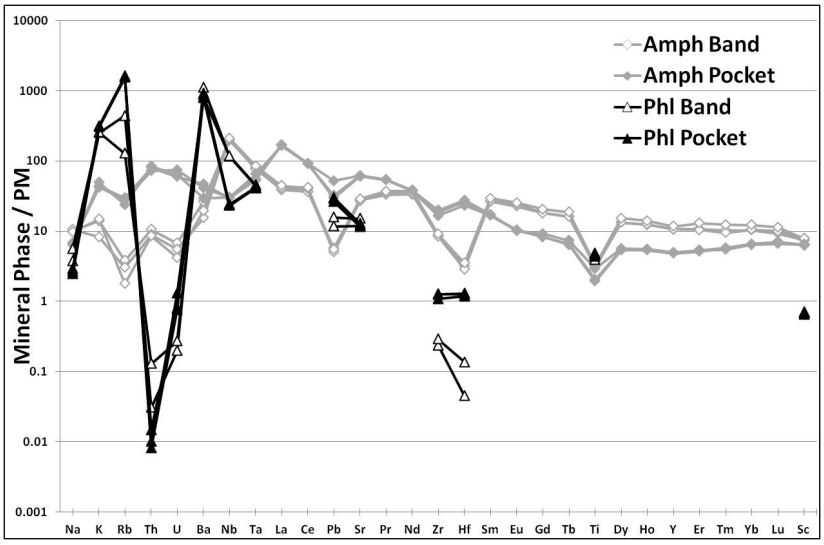

Figure 5. Primitive mantle (PM)-normalized trace-element patterns of phlogopite and amphibole from the phlogopite-bearing samples from Amph-Pd. Primitive mantle values are from Hofmann [29].

characterized by lower LREE content (La_N = 101–116) and higher HREE (Yb_N = 26.20–31.06).

The amphiboles from the two phlogopite-bearing lithologies differ also for other trace-element concentrations and fractionation (Figure 4b, values normalized to the Primitive Mantle, PM, reported by Hofmann [29]). The pocket amphibole has higher abundance in Rb, Th, U, Pb, Sr, Zr and Hf, but lower in Nb, Ta and Ti compared to the band amphibole (Figure 4b). Besides, pocket amphiboles have marked negative anomalies for Nb and Ta, with $Nb_N/Ta_N < 1$, but moderate or absent Zr and Hf anomalies, with Zr_N/Hf_N slightly lower than 1 (as typically observed in amphiboles segregated from primary melts; [30]). In contrast, band amphiboles display positive Nb and Ta anomalies, with $Nb_N/Ta_N < 1$, and pronounced Zr and Hf anomalies with $Zr_N/Hf_N > 1$ (Figure 4b). Both amphiboles exhibit negative anomalies for Pb and Ti which are more pronounced in the band. Th_N/U_N ratio is commonly higher than 1 (Table 3), with the exception of one crystal from the pocket with a ratio of 0.96 (Table 3).

5.2.2. Phlogopite

The band phlogopite commonly shows higher trace-elements abundance compared to the pocket phlogopite, with the exception of Rb, U, Pb, Zr and Hf (Figure 5, Table 2). Rb and Ba contents are higher than the associated amphiboles. Both phlogopite samples exhibit a negative Nb anomaly, which is less pronounced compared to that one of the coexisting amphibole.

The Zr_N/Hf_N ratio in the pocket is around 1 (0.92–1.01), whereas in the band has higher values (2.11–5.26, Table 3). A similar behavior is shown by the Th_N/U_N ratio (0.01–0.02 in the pocket and 0.16–0.48 in the band, respectively, Table 3). The Zr_N/Hf_N ratio of phlogopite is similar to that of one of the associated amphiboles, while the $(Th/U)_N$ ratio is slightly different.

6. Discussion

6.1. The nature of the geochemical differences between the two phlogopite-bearing occurrences

The occurrence of phlogopite in the Finero Mafic Complex is rare and essentially limited to small outcrops within the Amph-Pd unit: in particular, it is identifiable in a band (or lens), whose extension cannot yet be defined in detail, and in a small pocket. Phlogopite also occurs in the host peridotite of the latter, up to 6.7 cm from the contact.

In the band and in the host peridotite of the pocket, phlogopite is present in an interstitial position, and is often associated with amphibole (i.e. pargasite), mainly in recrystallization zones where the cumulate olivine crystals underwent grain size reduction with formation of small neoblasts in a mosaic texture. The hornblendite vein, associated with the pocket, is located in a deformation zone of the host peridotite, which shows a foliated texture characterized by the alignment of black spinel and neoblasts of olivine. This evidence suggests that the crystallization of the studied phlogopite-bearing rocks within the Amph-Pd

unit is due to late melt migration events that occurred at high T, concomitantly to a deformation regime affecting the Finero Mafic Complex. In particular, the parent melt of the pocket migrated into the peridotite and was emplaced in the focused conduits where a strong recrystallization occurred, while the parent melt of the band intruded pervasively via porous flow in this particular area of the Amph-Pd unit.

The mineral assemblages of the studied samples are characterized by the abundance of hydrous minerals (i.e. amphibole and phlogopite), which suggests that the parental melts of the phlogopite-bearing rocks in the Amph-Pd were rich in H_2O and alkalis. Moreover, the presence of phlogopite as a primary liquidus phase is a marker of high contents of K in the parental melts.

Geochemical data indicates that the parent melt of the pocket had to be more enriched in K, Rb, Th, U, Pb and Sr, but relatively depleted in Na, Nb, Ta, Ti and MREE-HREE with respect to the melt that produced the band (see the comparison of the composition of amphibole and phlogopite in Figures 3, 4a,b and 5, Tables 2 and 3). The parent melt of the pocket had also to be enriched in Si compared to the band melt, as attested by the abundant orthopyroxene within the pocket.

The differences in terms of field and petrochemical features of the two occurrences suggest that the formation of the phlogopite-bearing lithologies in the Amph-Pd was potentially related to two distinct intrusive events related to the migration of different parent melts under different rheological and/or stress conditions.

On the other hand, Tiepolo et al. [31] demonstrated that in Si enriched conditions and at high pressure HREE partition coefficients between amphibole and alkaline melts become compatible (> 1), while LREE still behave incompatibly. Thus, an amphibole-dominated fractional crystallization of Si enriched melts can induce strong LREE/HREE fractionation in the residual melts (see Fig. 11 in Tiepolo et al. [31]), with an increase of LREE accompanied by decreasing HREE. Such a fractionation trend matches the REE variations displayed by the amphiboles of the studied samples, assuming that the parental melt of the band was more primitive than the pocket melt. This process could also explain the relative depletion of $HFSE^{5+}$ and Ti in the pocket amphiboles, because they can be compatible in amphiboles precipitated from Si enriched liquids [32].

Thus, although the field and petrochemical features documented in this study point to pronounced differences in terms of rheological and stress conditions of melt intrusion and parent melt composition between the phlogopite-bearing rocks in the Finero Mafic Complex, a genetic link through amphibole-dominated fractional crystallization under Si enriched condition similar to that described by Tiepolo et al. [31, 32] cannot be ruled out.

6.2. Constraints on the relationships among different units of the Finero Mafic Complex

Siena & Coltorti [3] interpreted the Finero Mafic Complex as the result of fractionation of a single hydrous basaltic liquid of transitional affinity. In their model, based on bulk rock analyses, the formation of the Mafic Complex is attributed to a fractional crystallization process, with amphibole as an early liquidus phase after the segregation of plagioclase. Based on trace-element and isotopic data, Lu et al. [5, 6] proposed a tholeiitic MORB affinity for the parent melts, which possibly formed in depleted to slightly enriched mantle domains. Considering the correlation between $^{87}Sr/^{86}Sr$ ratio and K_2O and the very low bulk-rock U and Th contents, Lu et al [5, 6] suggested that the parent melts of the Finero Mafic Complex did not undergo contamination by crustal rocks.

However, petrographic evidence suggests that amphibole and phlogopite crystallized in these rocks during late processes of melt/fluid intrusions associated with the deformation of the cumulate sequence.

Very few data on the mineral chemistry of the Finero Mafic Complex are available in literature for comparison with our data. Lu et al. [5] report analyses for bulk rocks, while Siena & Coltorti [3] present only the average of major-element analyses for the mineral phases of each unit. Zanetti et al. [8] give the mineral chemistry of some EG gabbros composed of plagioclase, clinopyroxene, brown amphibole, orthopyroxene, ilmenite, magnetite and garnet. Although the differences in mineralogical associations can possibly exclude a direct relationship among the phlogopite-bearing samples studied and the EG rocks reported by Zanetti et al. [8], the latter are the only available compositional data of mineral phases from the Finero Mafic Complex.

Taken together, the EG mineral compositions of Zanetti et al. [8] differ from those of the pocket and band mainly in their lower Mg# and Cr_2O_3 content (Figure 3, Tables 1, 3 and 4). Conversely, the TiO_2 content of amphibole is higher (Figure 3, Tables 1, 3 and 4). The trace-element composition of amphibole shows a different geochemical affinity between the rocks studied here and those from the EG unit (Figure 4a,b). In particular, the EG amphiboles [8] have lower abundances for the highly incompatible elements (Th, U, Ba, Nb and Ta) and a negative anomaly for Sr (Figure 4b). Their REE patterns are depleted for LREE and flat from MREE to HREE for garnet-free samples, while garnet-bearing gabbros show fractionated patterns with depletion in HREE compared to MREE. Instead, the amphiboles studied here show patterns enriched in LREE and slightly fractionated from MREE to HREE (Figure 4a). Thus, the mineralogical, petrographic and geochemical differences between the phlogopite-bearing rocks and the

Table 4. Literature data comparison reported as phase averages and standard deviation (std. dev.).

Authors	Zanetti et al.					Zanetti et al.					Zanetti et al.		Siena & Coltorti			
Year	1999					1999					2013		1989			
Unit	Ph-Pd					Ph-Pd					EG		Amph-Pd			
Rock	Ap -bearing Ph Pd					Ap-free Ph Pd										
Phase	Amph	Opx	Phl	Ol	Sp	Amph	Opx	Phl	Ol	Sp	Amph	Opx	Amph	Opx	Ol	Sp
SiO_2 avg.	48.97	59.46	40.85	41.44	0.15	46.25	58.31	40.49	41.44	0.21	44.82	52.68	45.16	56.16	40.76	
SiO_2 std. dev.	0.59	0.86	0.95	0.23	0.11	0.73	0.37	0.87	0.38	0.06	1.18	0.73				
TiO_2 avg.	0.45	0.03	0.68		0.17	0.54	0.05	0.87	0.04	0.29	2.27	0.10	0.53	0.10		0.07
TiO_2 std. dev.	0.02	0.04	0.04		0.07	0.18	0.03	0.29	0.04	0.13	0.78	0.07				
Al_2O_3 avg.	7.26	0.27	13.74	0.02	5.29	11.15	0.99	15.51	0.03	19.34	11.10	1.85	12.18	2.67		42.64
Al_2O_3 std. dev.	0.45	0.02	0.57	0.02	0.48	0.76	0.25	2.19	0.04	1.74	1.51	0.93				
Cr_2O_3 avg.	2.34	0.19	1.42	0.02	57.67	1.97	0.29	1.20	0.00	43.81	0.08	0.02	0.98	0.31		16.47
Cr_2O_3 std. dev.	0.11	0.11	0.09	0.02	0.53	0.19	0.05	0.28	0.00	1.28	0.08	0.04				
FeO_T avg.	3.24	5.85	2.61	8.85	29.44	3.34	5.80	2.95	8.95	26.14	13.88	22.39	5.46	7.48	12.53	28.05
FeO_T std. dev.	0.18	0.41	0.21	0.45	1.68	0.16	0.19	0.25	0.27	2.64	2.82	0.87				
MgO avg.	20.17	35.42	24.13	49.77	6.16	19.33	35.48	25.09	50.50	10.32	11.33	21.24	16.83	32.70	46.23	13.24
MgO std. dev.	0.68	0.85	1.23	0.59	0.98	0.38	0.51	2.21	0.72	1.12	1.67	0.84				
Na_2O avg.	3.79	0.08	1.51			2.35	0.04	0.75			2.16					
Na_2O std. dev.	0.20	0.03	0.15			0.43	0.04	0.26			0.81					
K_2O avg.	0.56		6.95			0.78		7.58			0.69					
K_2O std. dev.	0.06		0.49			0.21		0.91			0.25					
Mg# avg	0.92	0.92	0.94	0.91	0.27	0.91	0.92	0.94	0.91	0.41	0.59	0.63	0.85	0.89	0.87	0.56
Mg# std. dev.	0.00	0.00	0.00	0.00	0.04	0.00	0.00	0.00	0.00	0.05	0.05	0.02				
$(La/Yb)_N$ avg.	4.12					18.69										
$(La/Yb)_N$ std. dev.	2.41					2.21										
$(La/Sm)_N$ avg.	1.38					2.76										
$(La/Sm)_N$ std. dev.	0.53					0.40										
$(Sm/Yb)_N$ avg.	2.82					6.85										
$(Sm/Yb)_N$ std. dev.	0.59					1.05										

EG samples suggest that the parental melt of the former is unrelated to the EG intrusion.

6.3. Comparison with the lithologies of the Ph-Pd unit

Presently, there is no evidence of a direct relationship between the parent melt of the Finero Mafic Complex and the melts that metasomatized the Ph-Pd unit. In particular, the parent melt of the Finero Mafic Complex has been assumed to be a hydrous MORB with tholeiitic-transitional affinity [3, 5, 8], whereas the metasomatism of the mantle unit occurred due to the migration of melt/fluid having a strong crustal slab-derived component [4, 7, 16–22, 33]. A possible genetic mismatch between the metasomatism of the mantle and the magmatic intrusion into the lower crust is also supported by the tectonic nature of the contact between the LIZ and Ph-Pd units.

However, ages reported in the literature for the Finero Mafic Complex intrusion event and the metasomatism of the Ph-Pd unit largely overlap. According to Zanetti et al. [8] and Gebauer [34] the intrusion of the EG unit occurred between 238–232 Ma (U-Pb SHRIMP zircon ages). Consistently, Lu et al. [6] determined ages ranging from 231 ± 23 Ma to 203 ± 13 Ma for the LIZ three- and two-point Sm/Nd internal isochrons. The LIZ three-point isochrons are closer to the older Triassic ages of the EG zircons, while the two-point Sm/Nd internal isochron from LIZ [6] shows younger ages (214 ± 17 Ma and 203 ± 13 Ma). Interestingly, Zanetti et al. [8] analyzed some recrystallized 'white pest' rims on magmatic zircons from the EG unit that provided younger discordant ages between 219 ± 3 and 205 ± 3 Ma, comparable with the younger ages reported by Lu et al. [6] for the LIZ. Zanetti et al. [8] suggested that the younger rim ages are the result of a fluid-assisted recrystallization event. This event was roughly associated with the injection of alkaline melts forming discordant dykes and pods within both the mantle and crustal Finero lithologies [35–40]. U-Pb analysis of zircons dates the intrusion of pegmatoid, nepheline-bearing alkaline dykes crosscutting the Mafic Complex at 226 ± 1.2 Ma [37, 38] and between 214–212 Ma [39].

For the mantle lithologies, ages obtained with different methods span between 240–163 Ma [4, 17, 21, 41–43]. In particular, Morishita et al. [21] determined a three-dimensional concordia isochron age of 215 ± 35 Ma (U-Pb SHRIMP data) in apatite from a vein within the Ph-Pd rocks, while Matsumoto et al. [42] obtained a 4-point isochron Ar/Ar age at 240 ± 41 Ma for the peridotite hosting the apatite-bearing vein. U-Pb zircon ages were performed to determine the crystallization age of the massive chromitites within dunite bodies inside the Ph-Pd unit [17, 43]. Conventional multigrain dating has been performed by von Quadt et al. [43], resulting in a concordant age of 204 ± 4 Ma with intercepts at 208 ± 4 to 207 ± 5 Ma. Analogous determinations by Grieco et al. [17] define an intercept age of 208 ± 2 Ma, but reveal the presence of an inherited component that plots, reverse discordant, at about 225 Ma.

In summary, both mantle and crustal rocks of the Finero Sequence show crystallization-recrystallization age intervals that strongly overlap and a possible relationship between them cannot be excluded.

The mineralogical assemblages of both the band and the pocket (amphibole + phlogopite ± orthopyroxene) would suggest a possible relationship with the metasomatizing melts/fluids that pervasively flowed through the Finero mantle unit. Metasomatism involved the extensive recrystallization and formation of new hydrous phases (amphibole + phlogopite). In fact, the metasomatic mineralogical association within the Ph-Pd, formed by pervasive crystallization of amphibole + phlogopite ± orthopyroxene in a depleted harzburgite [4, 7], is comparable to that one of the band and pocket in the Amph-Pd unit. Mineral compositions of the phlogopite-bearing amphibole harzburgite and associated phlogopite-bearing amphibole websterites of the Ph-Pd unit [7] show higher Mg#, SiO_2 and Cr_2O_3 contents compared to the minerals from the Amph-Pd unit (Figure 3, Tables 1, 3 and 4). The latter commonly has higher Al_2O_3 content than the Ph-Pd unit minerals, while only the pocket amphibole and phlogopite show high K_2O (Figure 3, Tables 1, 3 and 4).

The REE patterns of amphibole from the Ph-Pd unit [7] show similarities with those from the band and pocket (Figure 4a), but with lower element concentrations: they are enriched in LREE and fractionated to almost flat for the HREE. In particular, amphibole from Ph-Pd unit coexisting with apatite has REE patterns similar to those of the band amphibole, with almost-flat trends for LREE and HREE (Figure 4a), while amphibole from the apatite-free portions of the Ph-Pd unit shows similar highly LREE-MREE fractionated trends to the pocket amphibole (Figure 4a, La_N/Sm_N = 2.42–3.36 and 9.44–10.07, respectively) and the same slightly negative Eu anomaly (Eu_N/Eu_N^* = 0.78–1.02 and 0.80–0.88, respectively). Trace-element concentrations reflect the REE similarities (Figure 4a,b). Amphibole from apatite-bearing Ph-Pd [7] shows similar positive Nb and negative Zr and Ti anomalies as the band amphibole. They differ for the Rb absolute concentration (higher in the band amphibole) and for Sr, which is slightly enriched in the Ph-Pd compared to the Amph-Pd band. The band amphibole also shows higher abundance for other trace-elements, possibly related to melt fractionation. Similarly, but more pronounced, the trace-element concentrations in pocket amphibole are higher than the amphibole

from the apatite-free Ph-Pd unit [7]. Both minerals have negative Nb, Zr and Ti anomalies: Nb and Zr are less pronounced in the pocket amphibole while Ti is higher compared to the amphibole from the apatite-free Ph-Pd unit.

Similarities between the lithologies of the phlogopite-bearing Amph-Pd and the Ph-Pd units provide a possible relationship between the two events of (re)crystallization. In particular, the major- and trace-element mineral compositions suggest that the late melts intruding the Amph-Pd peridotites are similar to the metasomatizing melts/fluids in the Ph-Pd mantle unit, but more fractionated. The fractionation must have induced a depletion of SiO_2, Cr_2O_3 and MgO and enrichment of Al_2O_3, FeO and K_2O as revealed by major-element mineral composition (Figure 3, Tables 1 and 3).

The depletion in SiO_2 of the parent melt of the phlogopite-bearing Amph-Pd rocks provide for the absence of orthopyroxene in the early stage of crystallization (orthopyroxene does not occur in the band and is only present in the pocket but not in the parental hornblendite vein). Melt fractionation induced an enrichment of trace-element composition, which is higher in the phlogopite-bearing Amph-Pd rocks compared to those of the Ph-Pd mantle unit. This is mainly evident for the amphibole from the apatite-free Ph-Pd unit [7] and the pocket amphibole, while the band amphibole shows lower abundances for Rb and Sr compared to the apatite-bearing mantle samples. Although, the mineralogical and geochemical evidences suggest a possible relationship between the phlogopite-bearing Amph-Pd rocks and the metasomatized lithologies of the Ph-Pd unit, further isotopic analyses are required to constrain the origin of the Amph-Pd rocks.

7. Conclusions

This work presents new data on the Finero Mafic Complex. The occurrence of phlogopite, previously reported as 'rare' [2], is described in detail in two distinct occurrences within the Amph-Pd unit. The first of them represents a spatially uncertain band or lens, where phlogopite occurs as a secondary accessory phase mainly associated with amphibole. In this rock, based on petrographic and geochemical evidence, the amphibole-phlogopite association appears to be related to a late pervasive melt intrusion within a dunitic protolith. Phlogopite also occurs in a vein and pocket crosscutting the foliation in the peridotite of the Amph-Pd unit at a high angle. The vein and pocket are developed along a deformation zone within the peridotite. Within the vein, phlogopite is mainly associated with amphibole, while in the pocket the amphibole modal content decreases and orthopyroxene becomes the main mafic phase.

The mineral chemistry of these phlogopite-bearing lithologies within the Amph-Pd unit is different from other rocks of the Finero Mafic Complex and shares many similarities with the metasomatic mineralogical assemblage of the Finero mantle massif (i.e. the Ph-Pd unit). Therefore, we suggest a possible direct genetic relationship between the metasomatizing melts/fluids that recrystallized the Finero mantle massif and the parental melts of the phlogopite-bearing rocks in the Mafic Complex. We emphasize, however, that isotopic analyses are needed to verify this hypothesis, which, if confirmed, will provide new important constraints on the geodynamic evolution of the Finero area.

Acknowledgments

The constructive reviews by Lia N. Kogarko and three anonymous referees and the editorial handling of Michal Bucha and Lalou G. Gwalani have significantly improved the paper. We are very grateful to the Research Support Foundation of the State of São Paulo (FAPESP) and to the National Brazilian Research Council (CNPq) for financial support (FAPESP project 2013/19519-6).

References

[1] Cawthorn R.G., The amphibole-peridotite metagabbro complex, Finero, northern Italy. J. Geol., 1975, 83, 437-454

[2] Coltorti M. & Siena F., Mantle tectonite and fractionate peridotite at Finero (Italian Western Alps). Neues Jb. Miner. Abh., 1984, 149/3, 225-244

[3] Siena F. & Coltorti M., The Petrogenesis of a hydrate mafic-ultramafic complex and the role of amphibole fractionation at Finero (Italian Western Alps). Neues Jb. Miner. Monat., 1989, 6, 255-274

[4] Hartmann G. & Wedepohl K.H., The composition of peridotite tectonites from the Ivrea Complex, northern Italy: Residues from melt extraction. Geochim. Cosmochim. Ac., 1993, 57, 1761-1782

[5] Lu M., Hofmann A.W., Mazzucchelli M., Rivalenti G., The mafic-ultramafic complex near Finero (Ivrea-Verbano zone), I. Chemistry of MORB-like magmas. Chem. Geol., 1997a, 140, 207-222

[6] Lu M., Hofmann A.W., Mazzucchelli M., Rivalenti G., The mafic-ultramafic complex near Finero (Ivrea-Verbano zone), II. Geochronology and isotope geochemistry. Chem. Geol., 1997b, 140, 223-235

[7] Zanetti A., Mazzucchelli M., Rivalenti G., Vannucci R., The Finero phlogopite-peridotite massif: an example

of subduction- related metasomatism. Contrib. Mineral. Petr., 1999, 134, 107-122

[8] Zanetti A., Mazzucchelli M., Sinigoi S., Giovanardi T., Peressini G., Fanning M., SHRIMP U–Pb Zircon Triassic Intrusion Age of the Finero Mafic Complex (Ivrea–Verbano Zone, Western Alps) and its Geodynamic Implications. J. Petrol., 2013, 54/11, 2235-2265

[9] Zanetti A., Mazzucchelli M., Sinigoi S., Giovanardi T., Peressini G., Fanning M., Erratum. SHRIMP U–Pb Zircon Triassic Intrusion Age of the Finero Mafic Complex (Ivrea–Verbano Zone, Western Alps) and its Geodynamic Implications. J. Petrol., 2014, 55, 1239-1240

[10] Rivalenti G., Garuti G., Rossi A., The origin of the Ivrea-Verbano basic formation (western Italian Alps): whole rock geochemistry. B. Soc. Geol. Ital., 1975, 94, 1149-1186

[11] Rivalenti G., Rossi A., Siena F., Sinigoi S., The layered Series of the Ivrea-Verbano Igneous Complex, Western Alps, Italy. Tscher. Miner. Petrog., 1984, 33, 77-99

[12] Quick J.E., Sinigoi S., Mayer A., Emplacement of mantle peridotite in the lower continental crust, Ivrea-Verbano Zone, northwest Italy. Geology, 1995, 23/8, 739-742

[13] Quick J.E., Sinigoi S., Peressini G., Demarchi G., Wooden J., Sbisà A., Magmatic plumbing of a large Permian caldera exposed to a depth of 25 kilometers. Geology, 2009, 37/7, 603-606

[14] Sinigoi S., Quick J. E., Demarchi G., Peressini G., The Sesia Magmatic System. The Journal of the Virtual Explorer, 2010, 36.

[15] Correia C.T., Sinigoi S., Girardi V.A.V., Mazzucchelli M., Tassinari C.C.G., Giovanardi T., The growth of large mafic intrusions: Comparing Niquelandia and Ivrea igneous complexes. Lithos, 2012, 155, 167-182

[16] Zanetti A., Giovanardi T., Mazzucchelli M., Tiepolo M., Vannucci R., Morishita T., Pervasive migration of K-LILE-enriched melts through off-craton subcontinental lithospheric mantle: Sources, migration mechanisms and geodynamic environment. European Mineralogical Conference 2012, 2012, 1, 598

[17] Grieco G., Ferrario A., von Quadt A., Köppel V., Mathez A., The zircon-bearing chromitites of the phlogopite peridotite of Finero (Ivrea Zone, Southern Alps): evidence and geochronology of a metasomatized mantle slab. J. Petrol., 2001, 42/1, 89-101

[18] Grieco G., Ferrario A., Mathez E.A., The effect of metasomatism on the Cr-PGE mineralization in the Finero Complex, Ivrea Zone, Southern Alps. Ore Geol. Rev., 2004, 24, 299-314

[19] Selverstone J. & Sharp Z.D., Chlorine isotope evidence for multicomponent mantle metasomatism in the Ivrea Zone. EPSL, 2011, 310, 429-440

[20] Giovanardi T., Zanetti A., Mazzucchelli M., Tiepolo M., Vannucci R., Morishita T., Evidence for the development of a convergent setting in the Southern Alps domain during the early Mesozoic: insights from the Finero Complex (Ivrea-Verbano Zone). EGU General Assembly 2012 , Geophysical Research Abstracts, 2012, 14, EGU2012-14246

[21] Morishita T., Hattori K.H., Terada K., Matsumoto T., Yamamoto K., Takebe M., et al., Geochemistry of apatite-rich layers in the Finero phlogopite–peridotite massif (Italian Western Alps) and ion microprobe dating of apatite. Chem. Geol., 2008, 251, 99–111

[22] Morishita T., Arai S., Tamura A., Petrology of an apatite-rich layer in the Finero phlogopite–peridotite, Italian Western Alps; implications for evolution of a metasomatising agent. Lithos, 2003, 69, 37-49

[23] Raffone N., Le Fèvre B. L., Ottolini L., Vannucci R., Zanetti A., Light-lithophile element metasomatism of Finero peridotite (W Alps): A secondary-ion mass spectrometry study. Microchim. Acta, 2006, 155, 251-255

[24] Lensch G., Die Ultramafitite der Zone von Ivrea. Ann. Univ. Saraviensis, 1971, 9, 5-146

[25] Sills J.D., Ackermand D., Herd R.K., Windley B.F., Bulk composition and mineral parageneses of sapphirine-bearing rocks along a gabbro-lherzolite contact at Finero, Ivrea Zone, N Italy. J. Metamorph. Geol., 1983, 1, 337-351

[26] Sills J.D., Ackermand D., Herd R.K., Windley B.F., Bulk composition and mineral parageneses of sapphirine-bearing rocks along a gabbro-lherzolite contact at Finero, Ivrea Zone, N Italy. J. Metamorph. Geol., 1983, 1, 337-351

[27] Rivalenti G., Mazzucchelli M., Girardi V.A.V., Vannucci R., Barbieri M.A., Zanetti, A., et al., Composition and processes of the mantle lithosphere in Northeastern Brazil and Fernando de Noronha: evidence from mantle xenoliths. Contrib. Mineral. Petr., 2000, 138, 308-325

[28] Anders E. & Ebihara M., Solar system aboundances of the elements. Geochim. Cosmochim. Ac., 1982, 46, 2363-2380

[29] Hofmann A.W., Chemical differentiation of the Earth: The relationship between mantle, continental crust and oceanic crust. EPSL, 1988, 90, 297-314

[30] Tiepolo M., Bottazzi P., Foley S.F., Oberti R., Vannucci R., Zanetti A., Fractionation of Nb and Ta from Zr and Hf at Mantle Depths: The role of Titanian Pargasite and Kaersutite. J. Petrol., 2001, 42, 221-232

[31] Tiepolo M., Vannucci R., Bottazzi P., Oberti R., Zanetti A., Foley S., Partitioning of rare earth elements, Y, Th, U, and Pb between pargasite, kaersutite, and basanite to trachyte melts: Implications for perco-

lated and veined mantle. G^3, 2000, 1, paper number 2000GC000064

[32] Tiepolo M., Vannucci R., Oberti R., Foley S., Bottazzi P., Zanetti A., Nb and Ta in corporation and fractionation in titanian pargasite and kaersutite: crystal-chemical constraints and implications for natural systems. EPSL, 2000, 176, 185-201

[33] Downes H., Formation and Modification of the Shallow Sub-continental Lithospheric Mantle: a Review of Geochemical Evidence from Ultramafic Xenolith Suites and Tectonically Emplaced Ultramafic Massifs of Western and Central Eurore. J. Petrol., 2001, 42, 233-250

[34] Gebauer D., The Pre-Alpine evolution of the continental crust of the Central Alps: an overview. In: von Raumer, J.F., Neubauer, F. (eds) Pre-Mesozoic Geology in the Alps, Springer-Verlag, 1993, 93-117

[35] Stälhe V., Frenzel G., Kober B., Michard A., Puchelt H., Schneider W., Zircon syenite pegmatites in the Finero peridotite (Ivrea Zone): evidence for a syenite from a mantle source. EPSL, 1990, 101, 196-205

[36] Stähle V., Frenzel G., Hess J.C., Saupé F., Schmidt S.Th., Schneider W., Permian metabasalt and Triassic alkaline dykes in the Northern Ivrea Zone: clues to the post-Variscan geodynamic evolution of the Southern Alps. Schweiz. Miner. Petrog., 2001, 81, 1-21

[37] Klötzli U., Hochleitner R., Kosler J., Lower Triassic mantle-derived magmatism in the Ivrea-Verbano Zone: evidence from laser ablation U-Pb dating of a pegmatite from the eastern Finero Complex (Switzerland). Mitt. Osterr. Mineral. G., 2007, 153

[38] Klötzli U., Klötzli E., Günes Z., Kosler J., Accuracy of Laser Ablation U-Pb Zircon Dating: Results from a Test Using Five Different Reference Zircons. Geostand. Geoanal. Res., 2009, 33/1, 5-15

[39] Schaltegger U., Fanning C.M., Gunther D., Maurin J.C., Schulmann K., Gebauer D., Growth, annealing and recrystallization of zircon and preservation of monazite in highgrade metamorphism. Conventional and in-situ U-Pb isotope, cathodoluminescence and microchemical evidence. Contrib. Mineral. Petr., 1999, 134, 186-201

[40] Giovanardi T., Morishita T., Zanetti A., Mazzucchelli M., Vannucci R., Igneous sapphirine as a product of melt-peridotite interactions in the Finero Phlogopite-Peridotite Massif, Western Italian Alps. Eur. J. Mineral., 2013, 25 (1), 17-31

[41] Friedrichsen H., Hydration of the Finero Ultramafic body: Its origin and age. C.N.R. - D.F.G. Workshop "On the composition and structure of the lower continental crust", Varallo Sesia (VC, Italy). Abstracts Volume, May, 17th-20th 1989

[42] Matsumoto T., Morishita T., Masuda J., Fujioka T., Takebe M., Yamamoto K., et al., Noble gases in the Finero Phlogopite-Peridotites, ItalianWestern Alps. EPSL, 2005, 238, 130-145

[43] von Quadt A., Ferrario A., Diella V., Hansmann W., Vavra G., Köppel V., U-Pb ages of zircons from chromitites of the phlogopite peridotite of Finero, Ivrea Zone, N-Italy. Schweiz. Miner. Petrog., 1993, 73, 137-138

[44] Mazzucchelli M., Quick J.E., Sinigoi S., Zanetti A., Giovanardi T., Igneous evolutions across the Ivrea crustal section: The Permian Sesia Magmatic System and the Triassic Finero intrusion and mantle. Geological Field Trips, 2014, in press